Response of convection to relative sea surface temperature: Cloud-resolving simulations in two and three dimensions

S. Wang[1] and A. H. Sobel[1,2,3]

Received 16 November 2010; revised 4 February 2011; accepted 1 March 2011; published 15 June 2011.

[1] The properties of equilibrated tropical convection are studied using a cloud-resolving model with large-scale dynamics parameterized by the weak temperature gradient (WTG) approximation. Model integrations are performed in both 2-D and 3-D geometries. The target profile toward which horizontal mean free tropospheric temperature is relaxed is held fixed, while sea surface temperature (SST) is varied. Consistent with previous studies, large-scale ascent and precipitation increase under WTG as the SST is increased, but more rapidly in two dimensions than in three dimensions. This is related to greater extremes of near-surface buoyancy in two dimensions as well as a lower gross moist stability, and perhaps also to weaker entrainment. In both two and three dimensions, the vertical profiles of large-scale vertical velocity are top heavy and remarkably self-similar in shape as SST is increased. When all integrations are analyzed together, precipitation increases with column-integrated relative humidity once the latter reaches a threshold, as in observations and other models. However, within each integration, the two quantities are correlated negatively, albeit over a very narrow range.

Citation: Wang, S., and A. H. Sobel (2011), Response of convection to relative sea surface temperature: Cloud-resolving simulations in two and three dimensions, *J. Geophys. Res.*, *116*, D11119, doi:10.1029/2010JD015347.

1. Introduction

[2] Cloud-resolving models (CRMs; also known as cloud system-resolving models) are an increasingly important resource as we seek to understand the role of moist convection and its interaction with larger-scale dynamics. Though still limited by resolution and the need to parameterize some physical processes, CRMs at least partially resolve deep convection, avoiding the need for cumulus parameterization and thus presumably giving results more faithful to the behavior of the real atmosphere. It has recently even become feasible to run CRMs on global domains, though this remains sufficiently expensive that it is not a methodology in wide use. More common is to run a CRM on a limited domain representing a small region of the atmosphere with periodic boundary conditions in the horizontal. In this context, one can aim to examine the interaction between the convection (which is at least partly resolved) and larger-scale dynamics, which is represented in this context by domain-averaged quantities.

[3] The weak temperature gradient (WTG) approximation is a methodology that can be used to parameterize the large-scale vertical motion in a way broadly consistent with our understanding of large-scale tropical atmosphere dynamics. Otherwise, the large-scale vertical motion must be specified, which strongly constrains the domain-averaged convective activity. Under WTG, a CRM can be used to examine the bulk response of convection to external parameters such as sea surface temperature (SST) and surface fluxes (for example). Under specified large-scale vertical motion, these parameters will not exert a control on deep convection similar to that which they do in the real system under a fixed mean climate. Rather, under fixed large-scale vertical motion, a change in SST (for example) will cause a change in domain-averaged tropospheric temperature but little change in precipitation. Such a response may represent the effect of a change in SST due to a mean climate change, but not the effect of an SST variation (in space or time) for fixed mean climate. In the real tropical atmosphere where tropospheric temperature gradients must remain small, the free-tropospheric temperature profile can be thought of as related to the tropical mean SST [e.g., *Sobel et al.*, 2002]. Varying SST while holding free tropospheric temperature fixed (or relaxing it strongly to a target profile) can be thought of as varying the relative SST, or as the difference between the local and tropical mean SSTs [e.g., *Vecchi and Soden*, 2007; *Ramsay and Sobel*, 2011], and it is this relative SST that our simulations use as the primary control parameter.

[4] A number of studies have been performed with single-column models (SCMs) under WTG [*Sobel and Bretherton*, 2000; *Chiang and Sobel*, 2002; *Shaevitz and Sobel*, 2004; *Sobel et al.*, 2007; *Sobel and Bellon*, 2009; *Ramsay and*

[1]Department of Applied Physics and Applied Mathematics, Columbia University, New York, USA.
[2]Also at Department of Earth and Environmental Sciences, Lamont-Doherty Earth Observatory, Columbia University, New York, USA.
[3]Also at Lamont-Doherty Earth Observatory, Earth Institute of Columbia University, Palisades, New York, USA.

0148-0227/11/2010JD015347

Sobel, 2011]. A few have been performed with CRMs. These have used either an implementation similar to ours, but in two dimensions [*Raymond and Zeng*, 2005; *Raymond*, 2007; *Sessions et al.*, 2010], or a three-dimensional geometry, but with a different implementation of WTG, in which a one-dimensional wave equation is solved for the large-scale vertical velocity [*Kuang*, 2008; *Blossey et al.*, 2009; *Kuang*, 2011]; still, other studies have used related, but more different parameterizations of large-scale dynamics [*Mapes*, 2004; *Bergman and Sardeshmukh*, 2004]. In the present study, we use the Weather Research and Forecasting model (WRF) in both 2-D and 3-D configurations under WTG. Our goals are to determine whether key aspects of the results obtained in previous studies will be reproduced when a different model is used, to analyze some of those results in more detail, and, in particular, to examine the differences and similarities between 2-D and 3-D simulations.

[5] Past CRM studies [e.g., *Grabowski et al.*, 1998; *Tompkins*, 2000; *Phillips and Donner*, 2006; *Petch et al.*, 2008; *Stephens et al.*, 2008; *Wu and Guimond*, 2006] have found that, although some aspects of deep convection can be captured in a 2-D domain, 2-D convection may be distorted compared to that in a 3-D domain. These studies indicate that convection in two dimensions may exhibit excessive higher-frequency variability; time- and domain-averaged quantities such as temperature, relative humidity (RH), and bulk cloud microphysical properties may also be different in two dimensions than in three dimensions. *Bretherton and Smolarkiewicz* [1989] demonstrated that 2-D geometry artificially spreads the subsidence associated with a heat source, while *Tompkins* [2000] suggested that cold pools may be artificially enhanced in two dimensions. *Zeng et al.* [2007] showed that buoyancy is insufficiently damped in two dimensions such that excessive buoyancy oscillations are spuriously produced and further cause high-frequency variabilities, while *Petch et al.* [2008] showed that entrainment of dry air into convective cells in two dimensions is much weaker than in three dimensions; both effects favor stronger convection. Perhaps most dramatically, *Held et al.* [1993] showed that strong interactions between convection and the mean momentum field in two dimensions can lead, if not actively suppressed (e.g., by an imposed external restoring forcing on the horizontal wind field), to self-sustained long-period oscillations by a mechanism broadly similar to that of the stratospheric quasi-biennial oscillation. Whether these various distortions introduced by a 2-D configuration are acceptable depends on the situation and the question being asked. Understanding the capabilities and limitations of 2-D simulations is perhaps more relevant than in the past as 2-D CRMs are used in place of a convective parameterization in the multiscale modeling framework [*Khairoutdinov et al.*, 2005].

[6] The rest of this article is outlined as follows. Section 2 describes the details of the WTG implementation in WRF and the configurations of our numerical experiments. Section 3 presents results from a broad range of diagnostics applied to the experiments. Section 4 summarizes the conclusions.

2. Methodology

2.1. Weak Temperature Gradient

[7] We use the Advanced Research Weather Research and Forecasting Model version 3.0 [*Skamarock et al.*, 2008]. We have configured WRF to run under either the WTG or the radiative-convective equilibrium (RCE) mode in either 2-D or 3-D geometry. Our implementation of WTG has some minor differences in detail from that presented in previous studies, due to the particular vertical coordinate and configuration of WRF. Apart from these, it largely follows the work of *Raymond and Zeng* [2005] and *Sobel and Bretherton* [2000].

[8] The first step to implement WTG is to add a term representing large-scale vertical advection of potential temperature to the thermodynamic equation. This term is taken to relax the horizontal mean potential temperature in the troposphere to a prescribed profile:

$$\frac{\partial \theta}{\partial t} + \cdots = -\frac{\overline{\theta} - \theta_{RCE}}{\tau}, \tag{1}$$

where θ is potential temperature (or temperature), $\overline{\theta}$ is the mean potential temperature of the CRM domain (overbar indicates the CRM horizontal domain average), θ_{RCE} is the target potential temperature for the relaxation, and τ is the Newtonian relaxation time scale. When τ is taken close to 0 (a limit one may not be able to reach because of numerical issues), this becomes a strict implementation of WTG, and the horizontal mean free troposphere temperature must equal θ_{RCE}. In general, τ is interpreted as the time scale over which gravity waves propagate out of the domain, thus reducing the horizontal pressure and temperature gradients. Finite τ allows the temperature to vary in response to convective and radiative heating.

[9] The large-scale vertical circulation implied by this relaxation constraint is W_{wtg}, the WTG vertical velocity,

$$W_{wtg}\frac{\partial \overline{\theta}}{\partial \eta}(-\overline{\rho}g/\overline{\mu}) = \frac{\overline{\theta} - \theta_{rce}}{\tau}, \tag{2}$$

where ρ is the density, η is the dry mass-based vertical coordinate of WRF, and $-\overline{\rho}g/\overline{\mu}$ is part of the coordinate transformation from z to η; η is defined as $\eta = (p_d - p_d^T)/\mu$, where p_d is the dry pressure, p_d^T is a constant dry pressure at the model top, and μ is the dry column mass.

[10] Equation (2) implies the dominant balance in the tropics, i.e., adiabatic cooling by large-scale vertical motion tends to balance large-scale diabatic heating. In the CRM, the horizontal average over the domain of all other terms besides the tendency and relaxation terms in equation (1) would be considered diabatic heating from the point of view of a large-scale model with parameterized convection. Thus, in steady state, equation (1) implies that the dominant balance will hold with large-scale vertical motion parameterized by equation (2). Using the dry pressure differs from the conventional pressure coordinate, but it is numerically consistent and can be justified from the fact that the mass of the moisture in the troposphere is negligible (on the order $O(10^{-2})$) compared to the dry air mass. Within the boundary layer, following *Sobel and Bretherton* [2000], we do not apply equation (1) but instead obtain W_{wtg} by linear interpolation from surface to the planetary boundary layer (PBL) top. Unlike in previous studies, with our implementation of WTG, the PBL top is not fixed but is diagnosed in the boundary layer parameterization scheme (discussed below). The scheme determines a PBL top at each grid point, and we

use the maximum value in the computational domain at each time step as the PBL top for the computation of W_{wtg}.

[11] Transport of moisture by the large-scale motion introduces additional source and sinks for moisture. The moisture equation is updated at each time step by adding the following terms associated with the WTG vertical velocity:

$$\frac{\partial Q}{\partial t} + \cdots = -W_{wtg}\frac{\partial \overline{Q}}{\partial \eta}(-\overline{\rho} g/\overline{\mu}), \tag{3}$$

where Q is the moisture mixing ratio. The right-hand side of equation (3) is the advection by the large-scale vertical velocity W_{wtg}. Here we assume that the moisture field is horizontally uniform on large scales, such that the modeled convection is protected from the injection of reference profile humidities. *Raymond and Zeng* [2005] and *Sobel and Bellon* [2009] also incorporated parameterizations of the horizontal advection of moisture by large-scale flow. Raymond and Zeng's model assumes that the humidity of the air immediately surrounding the explicitly simulated convection is that of the reference profile, allowing parameterized horizontal advection by the large-scale divergent flow when the modeled domain's mean humidity differs from that of the reference. *Sobel and Bellon* [2009] modeled horizontal advection by relaxation toward a reference profile of zero humidity within a specified layer on a specified advective time scale (by a flow presumed entirely rotational, with horizontal advection by the divergent component neglected). While it can be represented different ways, qualitatively horizontal advection is expected to reduce the precipitation when it is large, assuming regions with large precipitation are among the most humid on the planet so that nearby ones are drier. Here we exclude this effect to simplify the parameter space but plan to explore it further in future work.

2.2. The WRF Model

[12] Here we briefly discuss the physical parameterization schemes used in this study. Boundary layer turbulence and the vertical subgrid scale eddy diffusion are treated with the Yonsei University (YSU) scheme [*Hong and Pan*, 1996; *Noh et al.*, 2003; *Hong et al.*, 2006). This is a first-order closure scheme but also includes the nonlocal counter gradient transport [*Troen and Mahrt*; 1986]. In this scheme, boundary layer height, a parameter also used in WTG, is determined by the local Richardson number, temperature and wind speed. The horizontal subgrid eddy mixing is parameterized using the 2-D Smagorinsky first-order closure scheme performed in physical space. The surface moisture and heat fluxes are parameterized following the Monin-Obukhov similarity theory. The bulk microphysics scheme is the Purdue-Lin scheme in WRF 3.1.1 [*Lin et al.*, 1983; *Rutledge and Hobbs*, 1984; *Chen and Sun*, 2002]. This scheme has six species: water vapor, cloud water, cloud ice, rain, snow, and graupel.

[13] Radiation is a simple Newtonian relaxation scheme as in the study by *Pauluis and Garner* [2006],

$$Q_R = \begin{cases} -1.5 \text{ K/d} & \text{for } T > 207.5 \text{ K} \\ \dfrac{200\ K - T}{5 \text{ days}} & \text{elsewhere} \end{cases}. \tag{4}$$

The troposphere is cooled at constant rate 1.5 K/d, which is close to the observed climatology. The stratospheric temperature is near constant 200 K. This radiative cooling has a very weak dependence on temperature. In the RCE and WTG experiments discussed below, the vertically integrated Q_R yields an energy loss of ~145 W/m^2 to the column, varying by no more than 1–2 W/m^2 (at very high SST). Hence, we can consider radiative cooling to be approximately fixed in our experiments. Such simple radiation cooling eliminates the complication of cloud-radiation feedback, so that only the parameterized large-scale circulation impacts the simulated convection and its organization. This simplifies the problem, at the cost of some loss of realism. In reality, long-wave radiative cooling can be suppressed by the abundant upper tropospheric ice cloud in the deep tropics, an effect that is absent in our results.

[14] WRF conserves dry mass to computer precision. However, conservation of moisture and energy are not guaranteed. Under RCE, in a sufficiently long time average, the surface moisture flux, E, should be exactly balanced by the precipitation, P, and the vertical integral of the radiative cooling $\langle Q_R \rangle$ should be exactly balanced by the sum of the surface latent heat flux (LE) and sensible heat fluxes (H): $\langle Q_R \rangle$ = LE + H. These balance constraints can be evaluated using model output from RCE integrations. When we do this, our choice of the above schemes leads to a relative error in the moisture budget $(P - E)/P \sim 0.5\%$, while the residual of the radiative cooling and the sensible and latent heat fluxes has relative error of ~1%. We consider these to be good results, but they are not independent of the choice of physics packages. Our tests showed that with different choices of physical parameterizations (such as eddy viscosity schemes, microphysics schemes, and boundary layer schemes), nonconservation of water vapor and energy can occur, with relative errors up to several tens of percent. Our choices of physical parameterizations were influenced in part by our desire to maintain good conservation properties.

2.3. Experiment Design

[15] Numerical experiments are performed in two and three dimensions under RCE and WTG. Statistical steady states are first achieved in RCE mode (no large-scale vertical advection applied in either temperature or moisture) over an SST of 28°C in both two and three dimensions. The time-averaged vertical temperature profile from these two experiments will be referred as the "reference" or RCE profiles. In our WTG integrations, SST is then varied from 27°C to 31.5°C while the horizontal mean potential temperature is relaxed toward the same RCE profiles in both two and three dimensions. Newtonian relaxation time scale τ in equation (1) is 3 h for all 2-D and 3-D experiments. Sensitivity experiments to this time scale is explored in section 3.7. The moisture field is integrated including advection by the implied large-scale vertical velocity as discussed above.

[16] The experiments are performed at the equator (the Coriolis parameter $f = 0$). We use 50 vertical levels with 10 levels in the lowest 1 km, while grid spacing is gradually stretched to 1.5 km near the model top (~22 km). The horizontal and vertical advections are fifth-order and third-order accurate, respectively. Moisture and other scalars are advected using a positive definite scheme [*Skamarock et al.*,

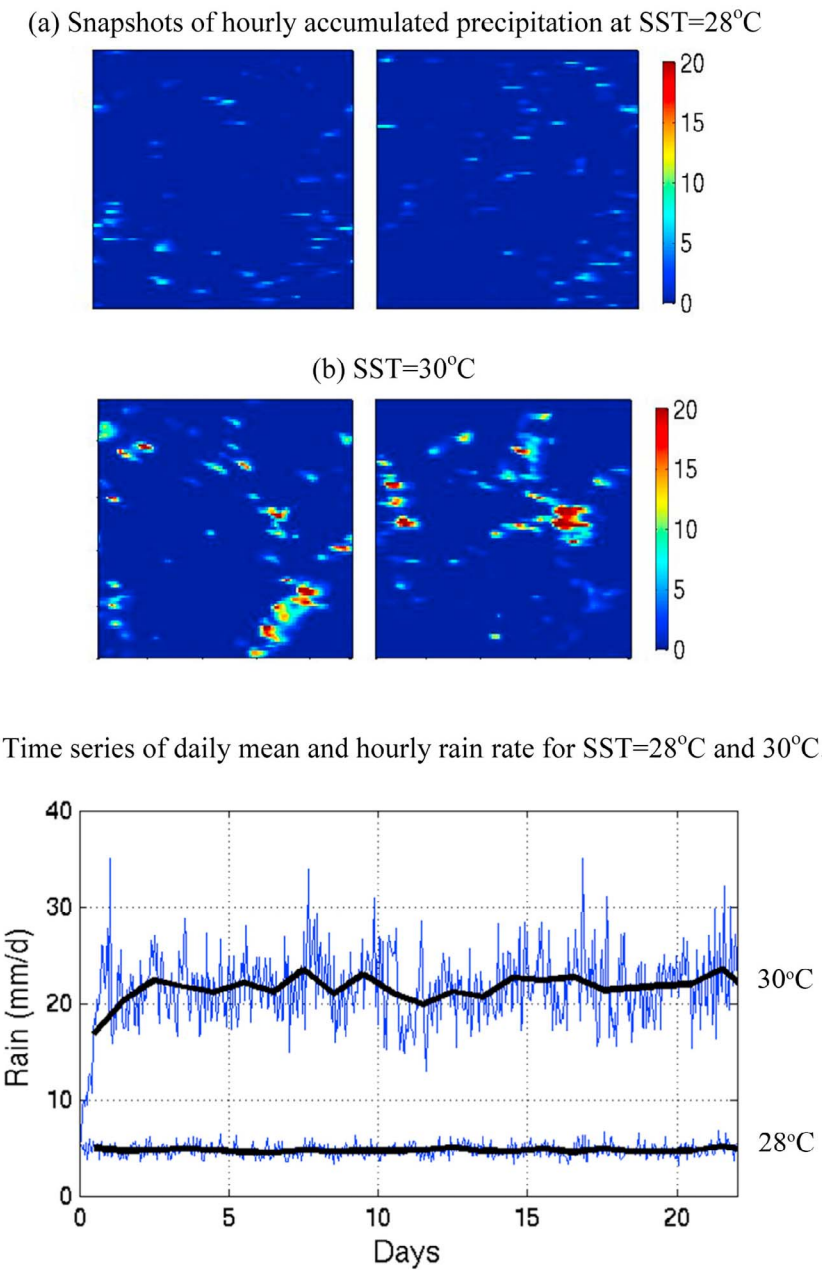

Figure 1. Snapshots of hourly precipitation in the 3-D WTG experiments for (a) SST = 28°C and (b) SST = 30°C. (c) Time series of daily (dark solid line, mm/d) and hourly (thin blue line, mm/d) rain rate for SST = 28°C and 30°C.

2008]. Vertically propagating gravity waves are absorbed in the top 5 km to prevent unphysical wave reflection off the top boundary by using the implicit damping vertical velocity scheme [*Klemp et al.*, 2008]. The horizontal grid spacing is 2 km. This horizontal resolution is close to that of the 2-D CRMs used in the multiscale modeling framework or "superparameterization" [e.g., *Khairoutdinov et al.*, 2005].

[17] The model domain has 96 × 96 horizontal grid points in the 3-D experiments. All the 2-D experiments are chosen to have the same horizontal grids as the 3-D experiments for a fair comparison between two and three dimensions under WTG. Our choice of the resolution and domain size is a result of the balance between high computational expense for long-term integrations and the desire to resolve both fine details and convective organization. We also perform experiments with a smaller domain size: 64 × 64 grid points and 32 × 32 horizontal grid points in three dimensions and 64 grid points and 32 grid points in two dimensions. The primary results are not sensitive to domain size within this range. It is possible that in sufficiently larger domains, convection would self-aggregate [*Bretherton et al.*, 2005], behavior that does not occur in our integrations.

[18] To avoid the pathological behavior of convective organization in 2-D geometry [*Held et al.*, 1993], the domain mean wind is relaxed to a vertically uniform value of 6 m/s with a relaxation time scale of 2 h for the 2-D experiments. Similarly, mean wind in one horizontal direction is relaxed for the 3-D experiments for the sake of fair comparison. The relaxation of mean wind also has some impact on the convection: it reduces the difference between two and three dimensions, because it strengthens winds in three dimensions (surface drag would otherwise eventually reduce the mean wind to near zero), while limiting the artificially strong perturbations in two dimensions, which would otherwise occur [*Tompkins*, 2000].

[19] The 3-D experiments under RCE are integrated for 6 months and the 2-D experiments for 8 months. The last 150 days are averaged to obtain the RCE state for three dimensions and last 300 days for two dimensions. The WTG experiments are integrated for 30 days for three dimensions and 120 days for two dimensions. The last 10 days of 3-D experiments and last 60 days of 2-D experiments are averaged to obtain the statistically steady state under relative SST forcing. Unless otherwise mentioned, diagnostics of vertical profiles are produced by averaging results for the last 10 days from the 3-D experiments and 150 days for the 2-D experiments. The longer sampling period for two dimensions is meant to partially compensate for the missing third dimension and accordingly reduced sample size in two dimensions.

[20] All the WTG experiments are initialized from one random snapshot of the RCE runs. Interestingly, previous studies have demonstrated that multiple equilibria are possible under WTG in both SCM [*Sobel et al.*, 2007] and CRM [*Sessions et al.*, 2010] integrations, given sufficiently different initial conditions. It is possible that for very dry initial conditions, some of our integrations that result in states with significant deep convection would instead reach dry states with no deep convection. This possibility is beyond the scope of the present study; our initial condition has sufficient moisture that we expect deep convection to occur unless the boundary conditions render it impossible, i.e., sufficiently low SST for a given target RCE temperature profile.

3. Results

3.1. Precipitation and Convective Organization Under WTG

[21] Precipitation in three dimensions is shown in Figure 1 for SST = 28°C and 30°C under WTG. The snapshots of hourly rain rates in Figures 1a and 1b are randomly sampled at two different times and indicate the spatial structure of convective organization. The impact of the relative SST is readily seen. There is virtually no organized convection at 28°C (also the SST for RCE runs) in these two snapshots. In contrast, at SST = 30°C, convection appears to aggregate and linear mesoscale convective systems (e.g., squall lines) are common. In fact, examination of the rain rate at other times indicates that there are always one to three well-organized convective clusters. To further quantify the impact of the relative SST on convection and precipitation, Figure 1c plots time series of the hourly and daily rain rate. At SST = 28°C, the daily rain rate remains approximately unchanged at the RCE value after WTG is turned on at day 0. At SST = 30°C, it increases smoothly during the first 5 days, after which it reaches a statistical equilibrium value of ~22 mm/d.

[22] Figures 2a and 2b show Hovmöller diagrams of the hourly rain rate at RCE and SST = 30°C in two dimensions. At SST = 28°C, there are a few bands of organized convection, as well as dry regions. At SST = 30°C, convective events are much more frequent while the dry region shrinks considerably. Cloud clusters appear to be able to propagate in both directions, although left-moving clusters are preferred, presumably because the mean wind is always close to 6 m/s. On the other hand, there is also no sign of organized cloud clusters in the Hovmöller diagrams from the 3-D experiments. Quantitatively, the rain rate at SST = 28°C (Figure 2c) is nearly steady, while it is much higher at SST = 30°C with increased variability. The daily rain rate reaches a statistically steady state ~32 mm/d after first 20 days at SST = 30°C. The 2 K increase of relative SST forces a much higher rain rate (~32 mm/d) in two dimensions than that (22 mm/d) in three dimensions. On the other hand, the rain rate at both hourly and daily time scales exhibits higher-frequency variability in two than in three dimensions, as first noted by *Grabowski et al.* [1998]. This greater temporal variability in two dimensions may be related to weaker damping of buoyancy in two dimensions, as suggested by *Zeng et al.* [2007], but may also be, to some extent, simply a result of sampling given the much smaller number of grid points used to compute daily rainfall in two dimensions.

[23] Figure 3 shows the equilibrated precipitation versus SST ranging from 27°C to 31.5°C for all the 2-D and 3-D experiments. In general, precipitation increases above 28°C and vanishes below 28°C. We will refer to these two regimes as the "wet" and "dry" regimes below, with the RCE state at 28°C falling between the two. We first briefly discuss the dry regime. In both the dry and wet regimes, the surface heat fluxes (latent plus sensible) are greater than those found at SST = 28°C, the RCE value. This may be induced by enhanced thermodynamic disequilibrium between the ocean and lowest model levels. It also has implications for the energy budget, as discussed in more detail in section 3.6. At SST = 28°C, the rain rates, as well as surface fluxes, for two and three dimensions are almost the same, around 4.8 mm/d. This illustrates that introducing WTG at the RCE SST does not cause the model to diverge from the RCE state; the RCE is robust in this sense, as has been found in some single-column models [*Sobel and Bretherton*, 2000, *Sobel and Bellon*, 2009], though not in the CRM calculations of *Raymond and Zeng* [2005] and *Raymond* [2007]. Nevertheless, the steady state in two dimensions under WTG is slightly drier than that in three dimensions. The rain rate is about 4.3 mm/d under WTG, nearly 10% lower than that in RCE.

[24] In the wet regime, rain rate and surface fluxes both increase with SST. The increases in surface heat fluxes in two and three dimensions are quantitatively very similar, while the increases in precipitation in two and three dimensions are qualitatively similar but quantitatively different. As noted above, at 2 K warming (30°C), P is ~22 mm/d for three dimensions and ~32 mm/d for two dimensions (Figure 3), nearly 60% more in two dimensions than in three

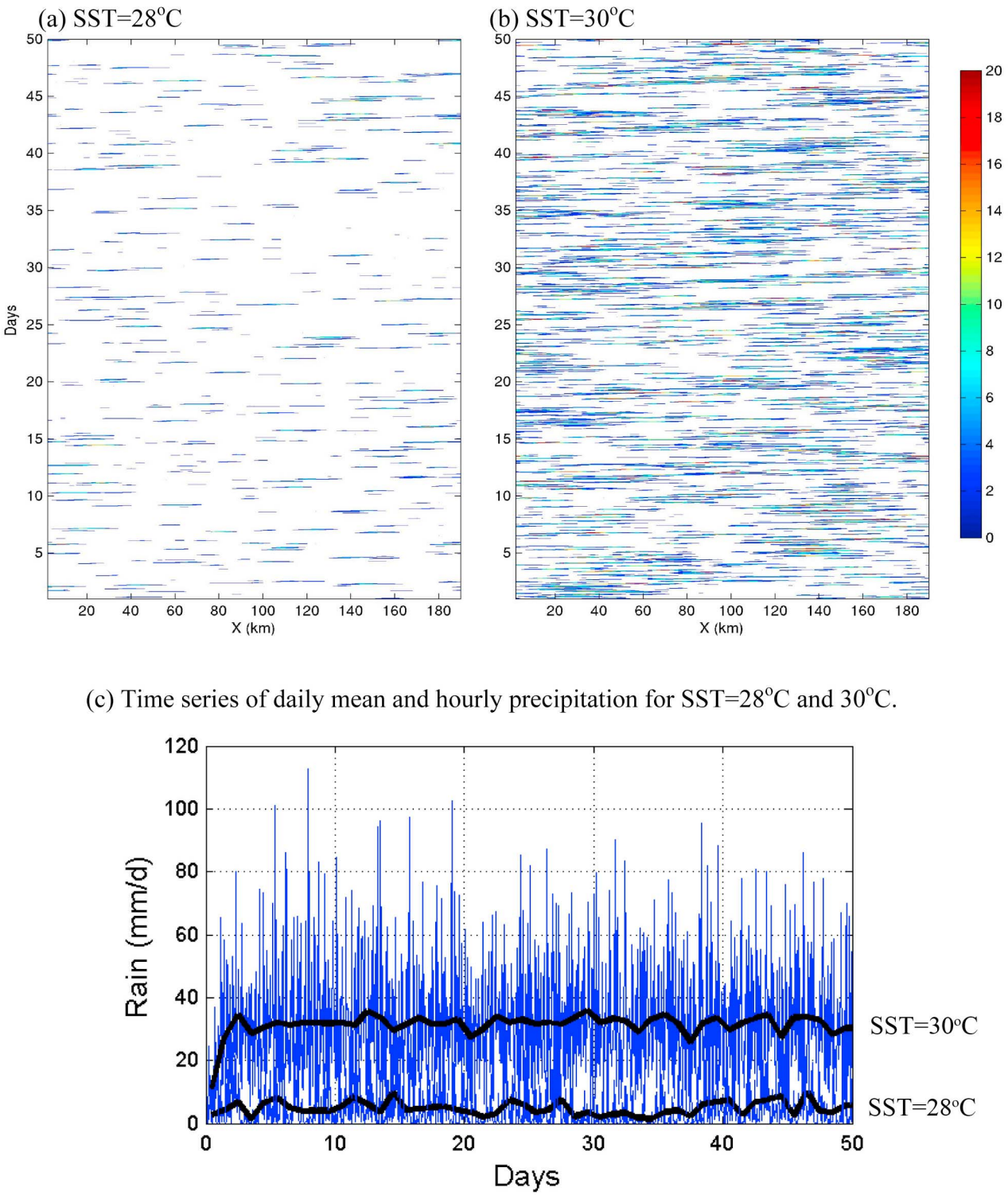

Figure 2. Hovmöller diagram of hourly precipitation in the 2-D WTG experiments for (a) SST = 28°C and (b) SST = 30°C. (c) Time series of daily and hourly rain rate (mm/d) for SST = 28°C and 30°C.

dimensions. The difference in precipitation cannot be attributed to surface fluxes, since those are similar; we show below (section 3.6) that instead the difference in precipitation is consistent with a smaller gross moist stability in two than in three dimensions.

3.2. Parameterized Large-Scale Circulation

[25] Figure 4 shows the large-scale vertical velocity W_{wtg} at statistically steady state under WTG for both two and three dimensions. W_{wtg} is top heavy for all SSTs greater than 28°C; at that value, W_{wtg} is close to zero, as expected.

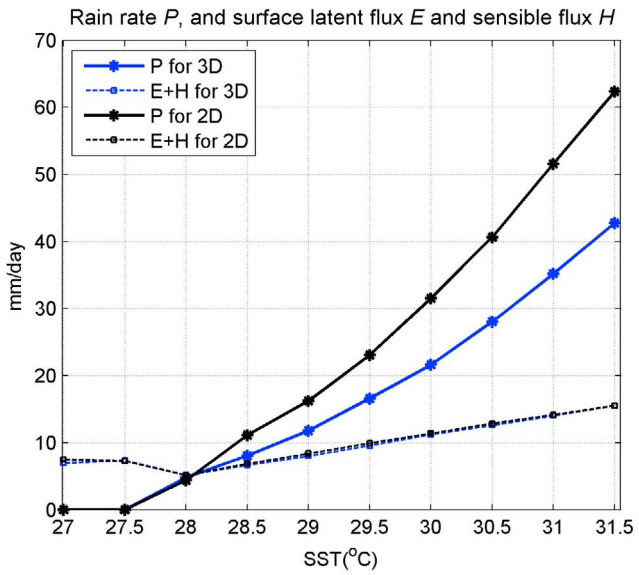

Figure 3. Daily rain rate P (mm/d, solid line) and surface fluxes (latent and sensible heat flux, E + H, in the unit of mm/d, dashed line) versus SST for two and three dimensions. Surface fluxes in three dimensions are almost the same as in two dimensions.

W_{wtg} peaks near 12 km. As SST increases further above 28°C, this peak value W_{wtg} also increases (Figure 4b): it reaches ~12 cm/s at SST = 30°C and ~25 cm/s at SST = 31.5°C in three dimensions. On the other hand, the shape of W_{wtg}, which is obtained by normalizing W_{wtg} by the peak value (Figure 4d), remains remarkably self-similar in all experiments despite substantial variation in the SST forcing.

[26] As SST is decreased below 28°C, precipitation ceases to occur. The dominant heat balance is between adiabatic warming by large-scale descent and radiative cooling. This explains why W_{wtg} is the same at dry SST regime 27°C and 27.5°C, as the radiative cooling is nearly identical in those two calculations.

[27] As documented by, for example, *Back and Bretherton* [2006, 2009], top-heavy, large-scale vertical velocity profiles are typical of the western Pacific warm pool region and bear self-similar vertical structure in the rainy regions [see *Back and Bretherton*, 2006, Figure 4]. In contrast to the self-similar shape of W_{wtg} in our model, *Kuang* [2011] obtained W_{wtg} profiles with a varying degree of top heaviness: as the scales of the coupled large-scale wave become smaller, W_{wtg} becomes more top heavy. We show below that variations in the W_{wtg} profile greater than those shown in Figure 4, and in some respects similar to those of *Kuang* [2011], can be obtained in our model by varying the relaxation time scale τ.

[28] On the other hand, our model in the present configuration does not produce any bottom-heavy profiles of W_{wtg}, such as are found in the east Pacific in reanalysis data sets [*Back and Bretherton*, 2006]. *Raymond and Sessions* [2007] obtained bottom-heavy W_{wtg} profiles by simultaneously warming the upper troposphere and cooling the lower troposphere in their target RCE temperature profile; when they used the unperturbed RCE profile from their model as the target, they obtained top-heavy W_{wtg} profiles qualitatively similar to ours.

[29] Although W_{wtg} behaves qualitatively similarly in response to the SST changes in two and three dimensions, there are significant quantitative differences. Figure 4b shows that W_{wtg} is significantly larger in two dimensions than in three dimensions at the same SST; its maximum value for 30°C (a 2 K warming in SST relative to the RCE value) is ~16 cm/s for two dimensions and ~12 cm/s for three dimensions. This is consistent with the rain rate difference between two and three dimensions at equilibrium states. How precipitation is related to W_{wtg} will be further discussed in detail through budget analysis of moist static energy in section 3.6.

3.3. Thermodynamic Structure

[30] In this section, we examine mean profiles of thermodynamic variables in the convecting atmosphere under WTG, including temperature, relative humidity, moist static energy, and buoyancy.

[31] Figure 5a shows the profiles of mean troposphere temperature (SST = 28°C) in both two and three dimensions. Variation of mean temperature under WTG with respect to the RCE profile is plotted in Figures 5a and 5b for three and two dimensions. In all the cases, unlike in strict WTG as has been enforced in some SCM studies [*Sobel and Bretherton*, 2000; *Ramsay and Sobel*, 2011], the free tropospheric temperature increases with SST, due to the finite relaxation time τ. T increases by 1.3 K in three dimensions and by 1.8 K in two dimensions at 2 K SST warming near 12 km, where latent heat release is maximum. *Ramsay and Sobel* [2011] showed in an SCM that upper troposphere can warm by ~5 K with 2 K increase in SST in RCE, because the temperature profile approximately follows a moist adiabat tied to the SST. So while warming in the upper troposphere under WTG in our model is quite different from zero, it is also considerably less than it would be in the RCE state given the same 2K SST perturbations as expected since WTG strongly inhibits upper troposphere warming. In the dry SST regime, free tropospheric temperature decreases as SST does, but the maximum decrease occurs near 1 km, the top of the boundary layer. This local minimum in temperature is associated with a deeper boundary layer, as seen from potential temperature profiles (not shown). Turbulence in the boundary layer maintains an approximately dry adiabatic temperature profile starting at the surface air temperature, which itself is close to the SST. When the SST is relatively low, the temperature just below the top of the PBL is cold compared to that above in the reference profile. In a deeper PBL, layers that were free tropospheric become part of the PBL and thus colder, resulting in the minimum around 1 km.

[32] Near-surface temperature increases weakly with SST, less than 0.5°C even with a 3.5°C SST (31.5°C) forcing, in contrast to ~2°C warming at upper levels. There is apparently a very strong negative feedback on near-surface air temperature, presumably due to convective downdrafts. A similarly strong negative feedback was found in the SCM calculations of *Ramsay and Sobel* [2011], who noted that the air-sea disequilibrium varies less with relative SST in simulations with global climate models than in the WTG SCM. We speculate that the strong negative feedback within

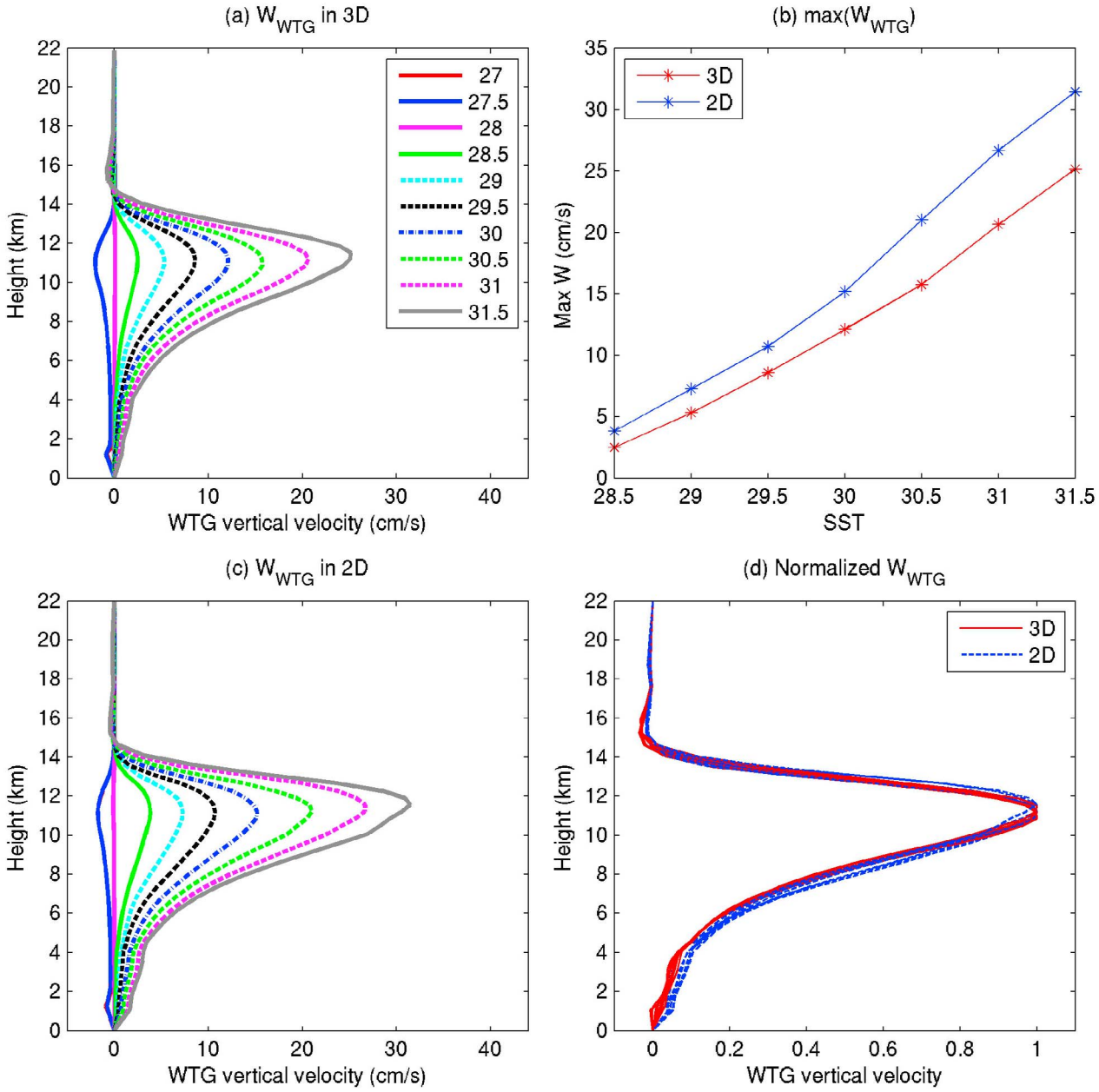

Figure 4. WTG vertical velocity for (a) three and (c) two dimensions. (b) The maximum value of WTG vertical velocity. (d) Normalized WTG vertical velocity.

the PBL in WTG calculations in both SCMs and CRMs may result from the quasi-steadiness of convection. In nature (and presumably in climate models) there is greater intermittency in the occurrence of deep convection, so that there are presumably periods without downdrafts when the boundary layer is able to recover more completely than in our WTG calculations.

[33] Here we show the association between enhanced convection at high SST and equivalent potential temperature θ_e in the subcloud layer, a rough indicator of parcel buoyancy at higher levels. Figure 6 plots the normalized histogram of θ_e at 100 m for SST $\geq$ 28°C. In both 2-D and 3-D experiments at RCE, θ_e values at 100 m are concentrated around the peak but are slightly skewed toward smaller values. In contrast to the left tail, the right tail of the histogram plummets to zero quickly a couple of degrees above the peak. At higher SST, the histograms are flatter. The distributions remain skewed toward smaller values, particularly in three dimensions. In two dimensions, the skewness becomes small at high SST. The increase of θ_e at high SST is associated with more frequent mesoscale convective systems as seen in both the 3-D and 2-D experiments (Figures 1 and 2).

[34] Figure 6c compares the θ_e distributions in the subcloud layer at 28°C and 30°C. At 30°C, the distribution has a slightly fatter right tail in two dimensions than in three dimensions, consistent with stronger convection as indicated

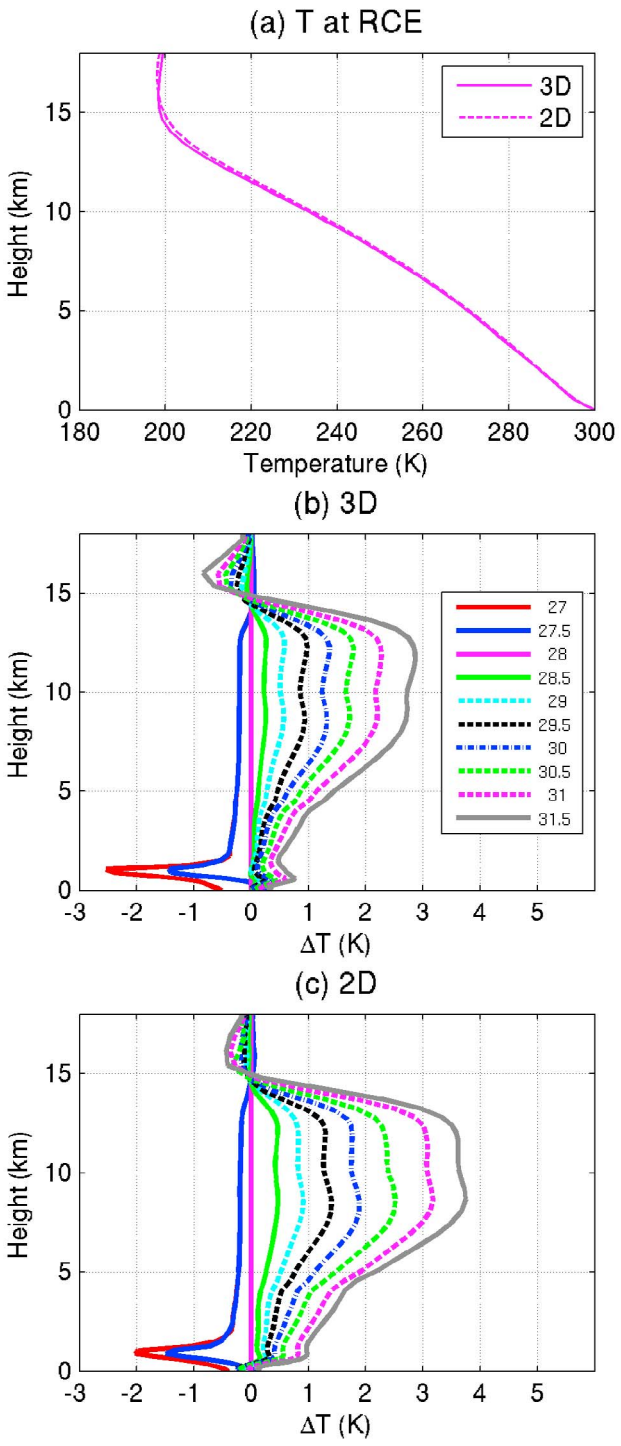

Figure 5. (a) Mean temperature from the 3-D and 2-D WTG experiments at 28°C. Temperature difference between all WTG experiments and the WTG experiment at 28°C for (b) three and (c) two dimensions.

by the difference in 2-D and 3-D rain rates at high SST shown above. *Tompkins* [2001] showed that cold pools were well formed and new convection can be initiated at the cold pool front even without mean wind shear. On the other hand, convection is also affected by the entrainment of less buoyant surrounding air into convective cells. Both factors, entrainment and cold pools, can be influenced by dimensionality. *Petch et al.* [2008] suggested that the entrainment rate was significantly larger in three dimensions than in two dimensions. It is not easy to quantify the relative roles of these two factors, and we do not attempt to do so here.

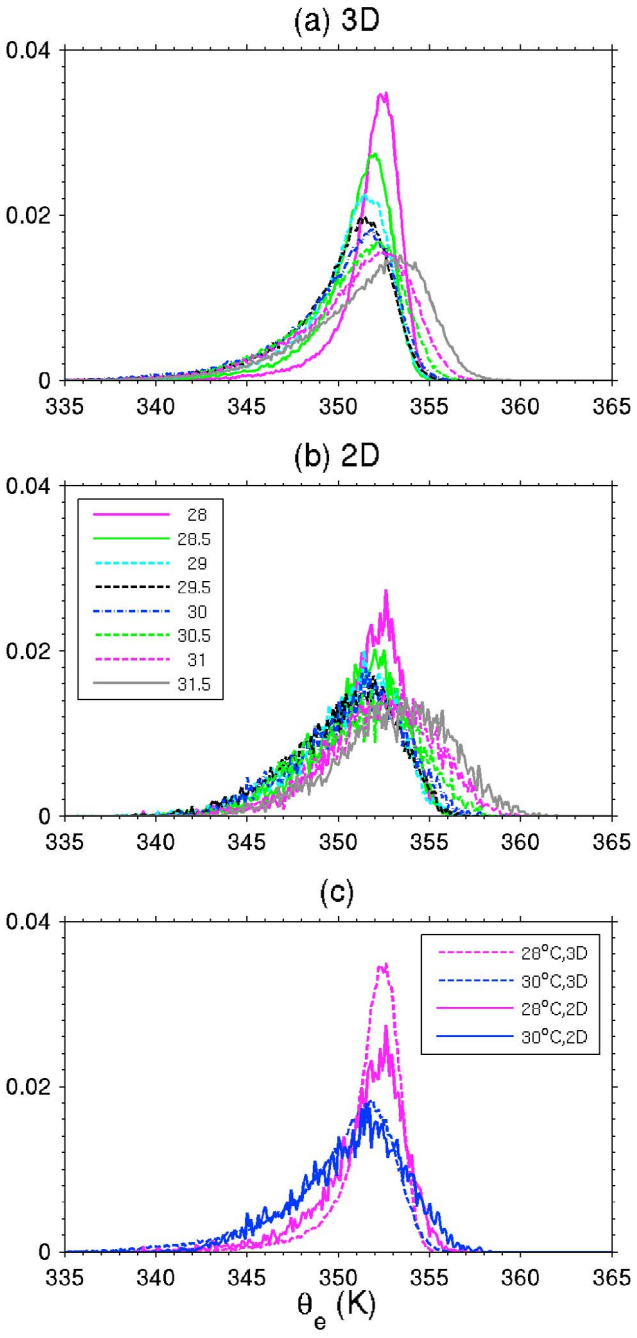

Figure 6. Normalized histogram of equilibrium potential temperature θ_e at 100 m for (a) three and (b) two dimensions. (c) Histogram of θ_e at SST = 28°C and SST = 30°C for three and two dimensions. Bin size of θ_e is 0.2 K. θ_e for SST less than 28°C is not shown.

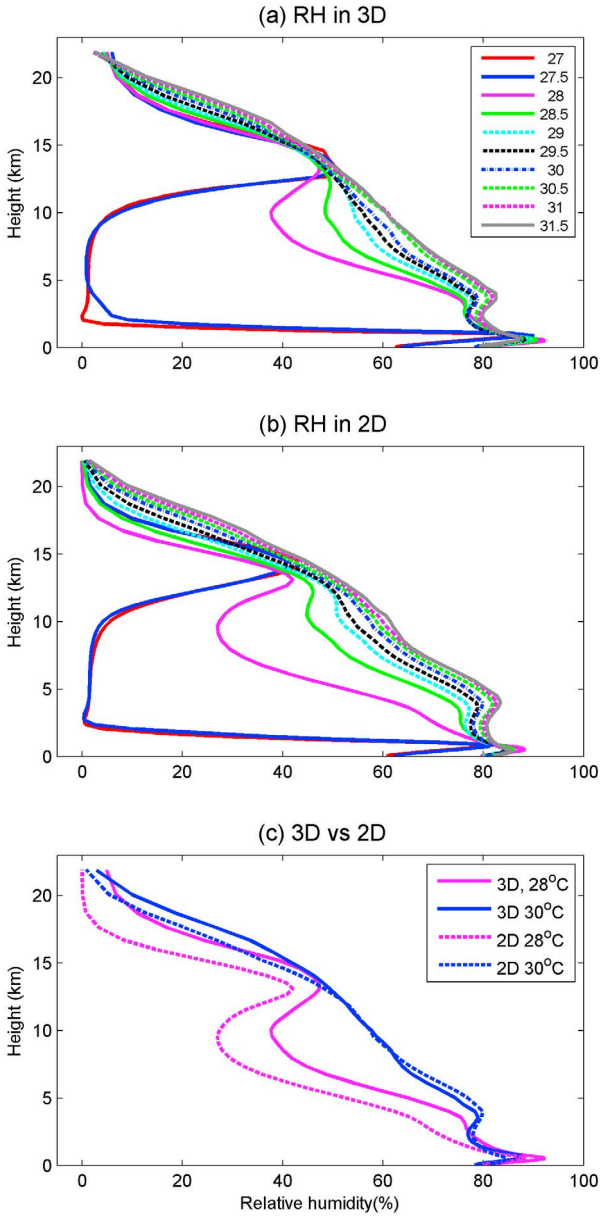

Figure 7. Relative humidity in (a) 3-D and (b) 2-D WTG experiments. (c) Relative humidity at SST = 28°C and 30°C for three and two dimensions is compared.

[35] Figure 7 displays relative humidity. RH at the RCE temperature is intermediate between the extremes of the dry and wet regimes. In the dry regime, free-tropospheric RH is near zero. This is as expected due to the lack of convective moistening to counteract the drying effect of large-scale descent and has been found in earlier WTG calculations with both SCMs and CRMs [e.g., *Sobel and Bretherton*, 2000; *Raymond and Zeng*, 2005; *Sobel et al.*, 2007; *Sessions et al.*, 2010]. In the wet regime, upper tropospheric RH increases rapidly with the first 1°C increase of relative SST but then saturates so that further SST increases only lead to slight increases in RH. The minimum just below 10 km, which is present at 28°C, is absent in the wet regime, in which the slope of RH with respect to height is nearly constant. This disappearance of the dry minimum is probably related to the enhanced vertical transport associated with enhanced convective fluxes. Compared to the SCM study by *Ramsay and Sobel* [2011, Figure 3b], the increase of RH at upper levels is greater here; in their SCM integrations, the RH minimum remained present at higher SST.

[36] Figure 7c compares RH at RCE and 30°C. In RCE, the 2-D integration has a significantly drier free troposphere than does the 3-D one. In the boundary layer, both temperature and moisture are very similar in two and three dimensions. At 30°C, the difference in RH between two and three dimensions is much smaller. It is slightly moister below 8 km in two dimensions. The relation between RH and precipitation will be discussed further below.

[37] Figure 8 shows vertical profiles of moist static energy

$$h = C_p T + gz + L_v Q. \tag{5}$$

Definitions of symbols are standard; h is approximately conserved during phase changes (without considering ice). At RCE, h is lower in two dimensions at its minimum (~5 km), probably because of the drier mean atmosphere and more cloud at lower atmosphere (Figure 9). In response to SST forcing, h increases with SST throughout the free troposphere in the wet regime. The minimum value (like the

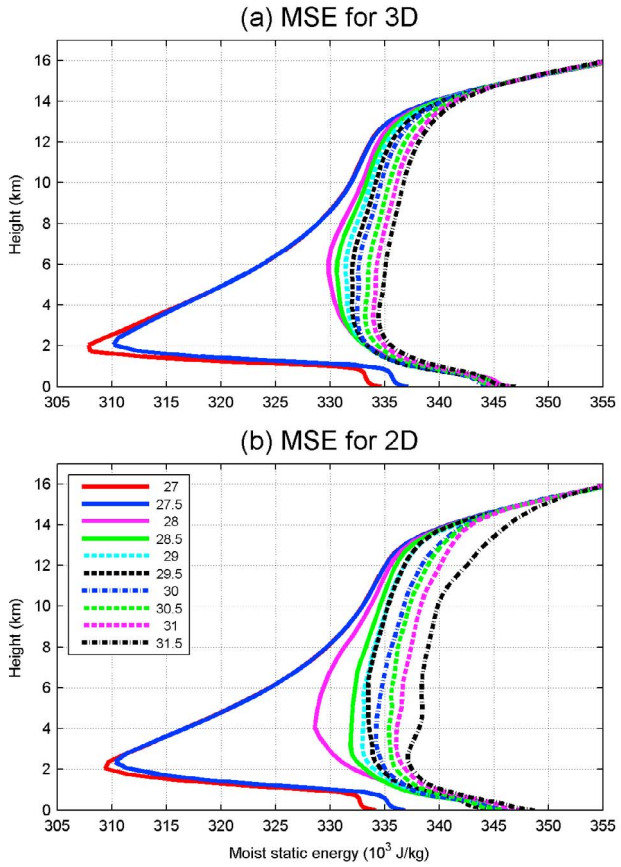

Figure 8. Moist static energy in all the (a) 3-D and (b) 2-D WTG experiments.

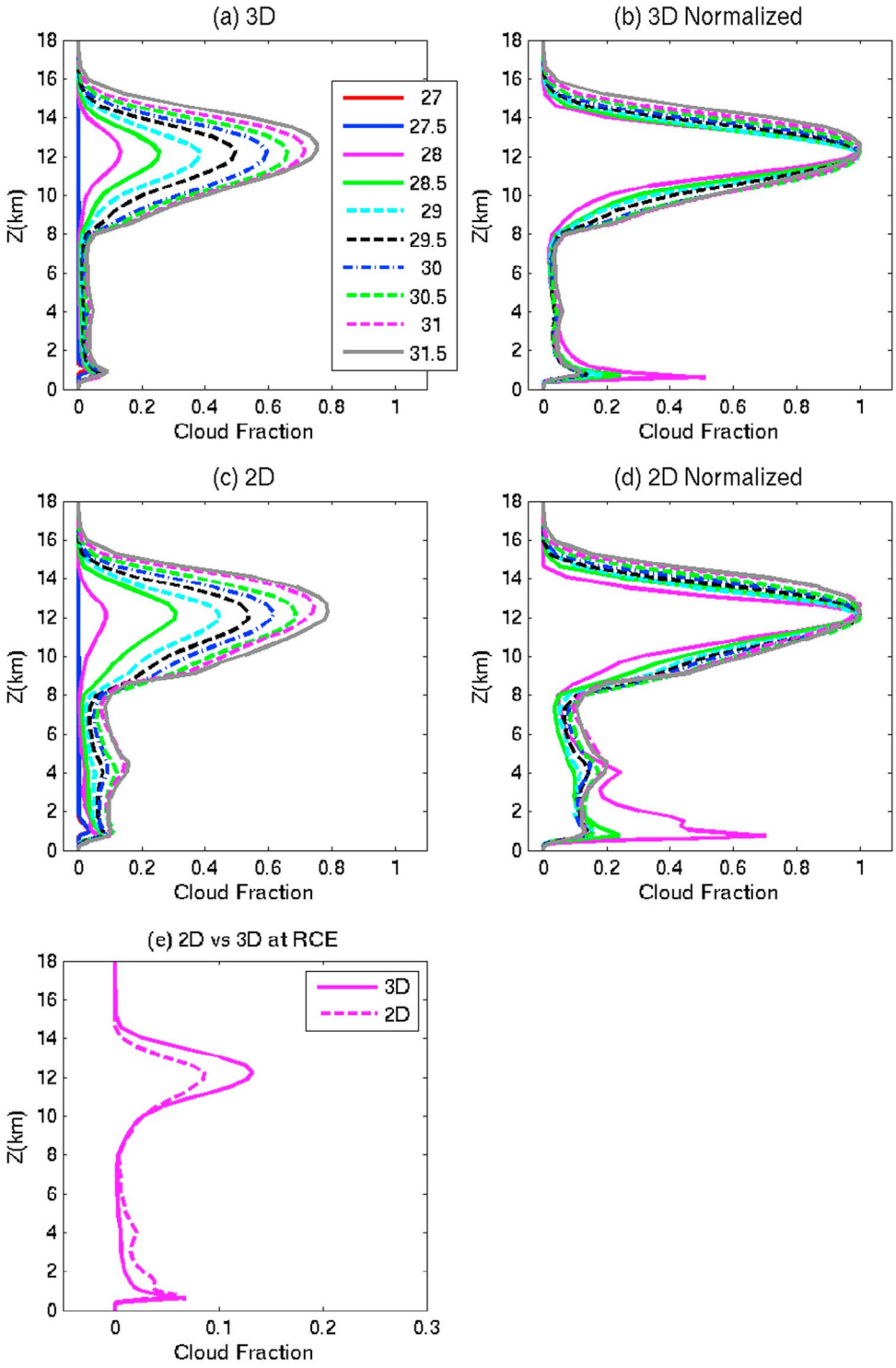

Figure 9. Cloud fraction in (a) 3-D and (b) 2-D WTG experiments. (b and d) Normalized cloud fraction of Figures 9a and 9c. (e) Cloud fraction at SST = 28°C. Cloudy points are chosen if cloud water q_c and cloud ice q_i is greater than 0.005 g/kg.

whole profile) increases with SST and becomes a rather shallow minimum; however, it occurs at a lower altitude (~3 km) at high SST than at RCE. Dry static energy behaves similarly to temperature under WTG with a maximum increase near 12 km (not shown).

3.4. Cloud Properties: Cloud Fraction and Convective Mass Fluxes

[38] Here we turn our attention to bulk cloud properties under WTG. Previous studies using CRMs with traditional forcing methods have noted that bulk cloud properties are

different in 2-D and 3-D experiments [e.g., *Tompkins*, 2000; *Phillips and Donner*, 2006; *Petch et al.*, 2008]. We find that the difference increases with relative SST under WTG.

[39] Cloud fraction is shown in Figure 9. The cloud is defined as the set of grid points where the mixing ratio of cloud hydrometeors (ice and water) is greater than 0.005 g/kg. At SST = 28°C, cloud fraction peaks at two levels, near 1 and 12 km, in both two and three dimensions. These two peaks indicate shallow and deep cumulus. There is also an indication of midlevel cloud near the melting level (~4 km; see Figure 5a). Compared to 3-D experiments, the 2-D RCE experiments have more shallow and midlevel cloud but less deep cloud.

[40] Under WTG, cloud fraction in the upper troposphere increases quickly with SST, more rapidly in two than in three dimensions. It increases from 0.07 at 28°C to 0.6 at 30°C in two dimensions and from 0.12 at 28°C to 0.55 at 30°C in three dimensions. Below 2 km, there is a small increase in cloud fraction with SST in three dimensions but much more in two dimensions.

[41] The profile of cloud fraction is normalized by the maximum value (Figures 9b and 9d), as was the WTG velocity in Figure 4. Unlike the self-similar structure of W_{wtg}, cloud fraction shows more variations in the low and mid troposphere, particularly for two dimensions. Low cloud (below 2 km) is much less at large SST.

[42] Convective mass fluxes are key quantities for a statistical description of convection. Here we examine both updraft (M_u) and downdraft (M_d) mass fluxes. M_u is estimated, similarly to *Robe and Emanuel* [1996], as the sum over the points with positive liquid water content greater than 0.005 g/kg and vertical velocity greater than +1 m/s, normalized by total number of grid points,

$$M_u = \sum\nolimits_{q_c>0.005g/Kg, w>1m/s} \rho_{i,j} w_{i,j}/N, \tag{6}$$

where i and j indicate grid points, ρ is density, and N is the total number of horizontal grid points. Downdraft mass flux M_d is estimated over points where $w < -1$ m/s; no threshold on liquid water content is applied as we are interested in unsaturated as well as saturated downdrafts.

[43] Figure 10 shows M_u and M_d for all experiments with SST greater than or equal to 28°C. At the RCE SST, M_u is larger at lower levels than at upper levels. At lower levels, M_u is slightly larger in three dimensions than in two dimensions. M_u increases rapidly with SST; the increase is more rapid in two than in three dimensions, consistent with the results for precipitation. The absolute value is much higher than that found in the SCM of *Ramsay and Sobel* [2011], but this may be partly due to the threshold used here, which is necessarily somewhat arbitrary.

[44] Updraft mass flux M_u does not always peak in the upper troposphere, as does cloud fraction and WTG velocity. In RCE (28°C), it peaks at ~2 km, suggesting a greater role for shallow convection. Figures 10b and 10d show convective mass flux normalized by its peak value, which clearly reveals the difference between the shallow and deep convection. Like cloud fraction, convective mass flux is not self-similar. As SST increases above RCE, convective mass flux becomes more top heavy with relatively less mass flux in the low troposphere.

[45] Downdraft mass flux M_d generally peaks at heights near those where updraft mass flux M_u does. Comparing Figures 10a and 10c suggests that M_d is stronger in two dimensions than in three dimensions. Here we quantify the relative strength of M_d to M_u using the ratio M_d/M_u. M_d/M_u at the top of boundary layer is an important parameter in the theory of boundary quasi-equilibrium [*Emanuel*, 1995; *Raymond*, 1995; *Raymond et al.*, 2009]. In our WTG experiments, M_d/M_u at 1 km (close to top of boundary layer) is 0.75 for two dimensions and 0.35 for three dimensions at SST = 28°C. At SSTs greater than 28°C, it is 1.0–1.5 for two dimensions and 0.4–0.6 for three dimensions. This ratio varies, however, with the w threshold chosen in equation (6). Figure 10f shows M_d/M_u decreases from 2 to 5 to zero as threshold value of w increases from 0 to 3 m/s, as M_d decreases more rapidly with larger w threshold than does M_u. (Note that the ratio does not reach unity for a w threshold of zero because of the condensate threshold applied to M_u but not M_d. If no condensate threshold is applied to either one, the ratio does reach unity for a w threshold of zero (not shown), reflecting the fact that the WTG vertical velocity appears only in the thermodynamic budgets and not in the mass budget, so that the domain-averaged mass flux resolved by the model must vanish at each level.) The ratio in two dimensions is distinctly larger than in three dimensions for all w thresholds and all SSTs.

3.5. Precipitation and Column Relative Humidity

[46] Observational studies [*Bretherton et al.*, 2004; *Peters and Neelin*, 2006; *Neelin et al.*, 2009; *Holloway and Neelin*, 2009] have shown relationships between precipitation and the column relative humidity (CRH; the column-integrated water vapor divided by its saturation value). Theoretical and modeling studies have also examined the implications of these relationships [e.g., *Raymond*, 2000; *Raymond and Zeng*, 2005; *Sobel and Bellon*, 2009; *Muller et al.*, 2009]. Here we examine such relationships in our experiments.

[47] Figure 11 illustrates the daily rain rate versus column relative humidity at two different periods: the latter portions of the calculations, during which a statistical equilibrium is reached for any particular SST, and the earlier portions, which are transition periods from RCE to the new equilibrium. The equilibrium periods are sampled during the last 10 days for three dimensions and the last 30 days for two dimensions. The transition periods are sampled during the first 10 days for three dimensions and the first 30 days for two dimensions after WTG is switched on. Analysis is performed based on daily accumulated quantities as well as hourly quantities. The latter leads to similar mean relationships but greater spread, as expected.

[48] Compact relationships qualitatively similar to those seen in observations and other models are found between the daily rain rate and CRH for both periods. There is virtually no precipitation for CRH < 0.6, followed by a very sharp increase for CRH greater than 0.6. In the transition period (Figures 11a and 11b), two differences between two and three dimensions emerge. First, considerable spread of CRH and precipitation is seen in two dimensions. Also, the rain rate reaches greater values in two dimensions, consistent with the other statistics discussed above. The transition from near-zero precipitation to rapidly increasing precipitation with CRH also appears sharper in three than in two

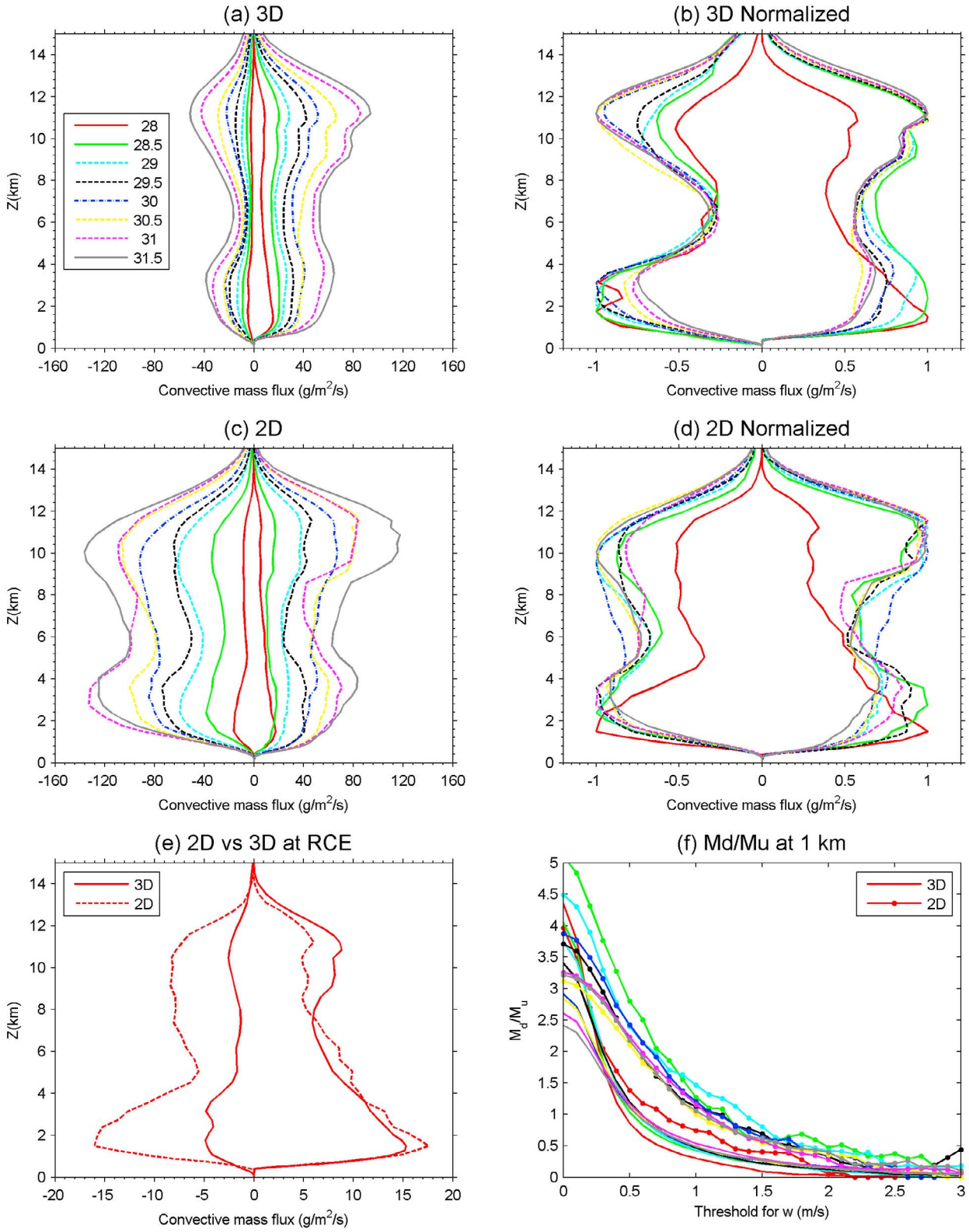

Figure 10. Updraft and downdraft mass flux in (a) 3-D and (c) 2-D WTG experiments for SST no less than 28°C. (b and d) Normalized convective mass flux of Figures 10a and 10c. (e) Convective mass flux at RCE (28°C). (f) Updraft mass flux is estimated on cloudy grid points (where qc + qi > 0.005 g/kg) with $w > 1$ m/s, and downdraft flux is estimated on points where $w < -1$ m/s shows M_d/M_u (the ratio between downdraft and updraft mass flux) at 1 km for SST no less than 28°C as the w threshold varies from 0 to 3 m/s.

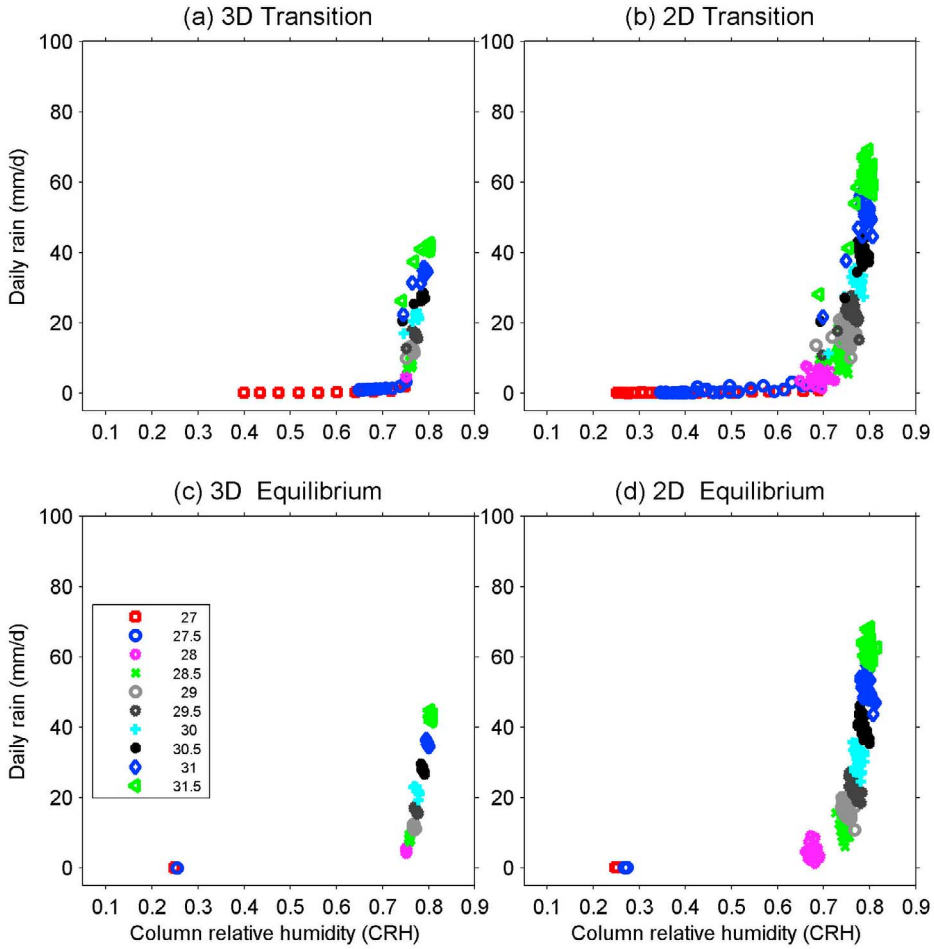

Figure 11. Daily rain rate versus column relative humidity for three (Figures 11a and 11c) and two dimensions (Figures 11b and 11d). (a and b) Data at the transition periods from RCE to WTG (sampled for the first 10 days for three dimensions and first 30 days for two dimensions). (c and d) Data at the equilibrium periods of WTG (sampled for the last 10 days for three dimensions and the last 30 days for two dimensions).

dimensions, though it is possible that this is a result of greater scatter in two dimensions.

[49] In the equilibrium period (Figures 11c and 11d), we still have compact relationships between CRH and precipitation similar to those in the transition period. However, a fine-scale feature emerges somewhat more clearly. For any given integration at a particular SST, the rain rate decreases slightly with respect to CRH, contrary to its general increase with respect to CRH when multiple integrations with different SST are considered together. The spread of precipitation appears to be larger at higher CRH. The decline of precipitation with CRH at constant SST presumably reflects negative feedbacks between the two variables, such as the drying effect of precipitation. We have not investigated this further, but there could be useful clues here about the mechanisms responsible for the overall CRH-precipitation relationship.

[50] We have also examined the rain rate accumulation at shorter time scales (e.g., 6 h). This substantially increases the sample size of rain rate in three dimensions (by a factor of 4 compared to daily sampling). All the features discussed above and the difference between two and three dimensions still hold, suggesting that it is unlikely the small sample size (10 days from each experiment) in three dimensions is an issue for the features discussed above.

3.6. Budget Analysis

[51] In our experiments, precipitation increases nonlinearly with respect to the SST forcing (Figure 3), confirming earlier results from single-column models [*Sobel and Bretherton*, 2000; *Ramsay and Sobel*, 2011], both qualitatively and quantitatively: 2 K warming leads to 4–5-fold increase of daily rain rate. Here we analyze the moist static energy budget in order to understand the controls on precipitation in more detail.

[52] The budgets of vertically integrated moist static energy (h) and dry static energy (s, similar to h but without the moisture term in equation (6)) in the statically steady state can be written as

$$\langle w\frac{\partial s}{\partial z}\rangle = H + P + \langle Q_R\rangle \text{ and } \langle w\frac{\partial h}{\partial z}\rangle = E + H + \langle Q_R\rangle, \qquad (7)$$

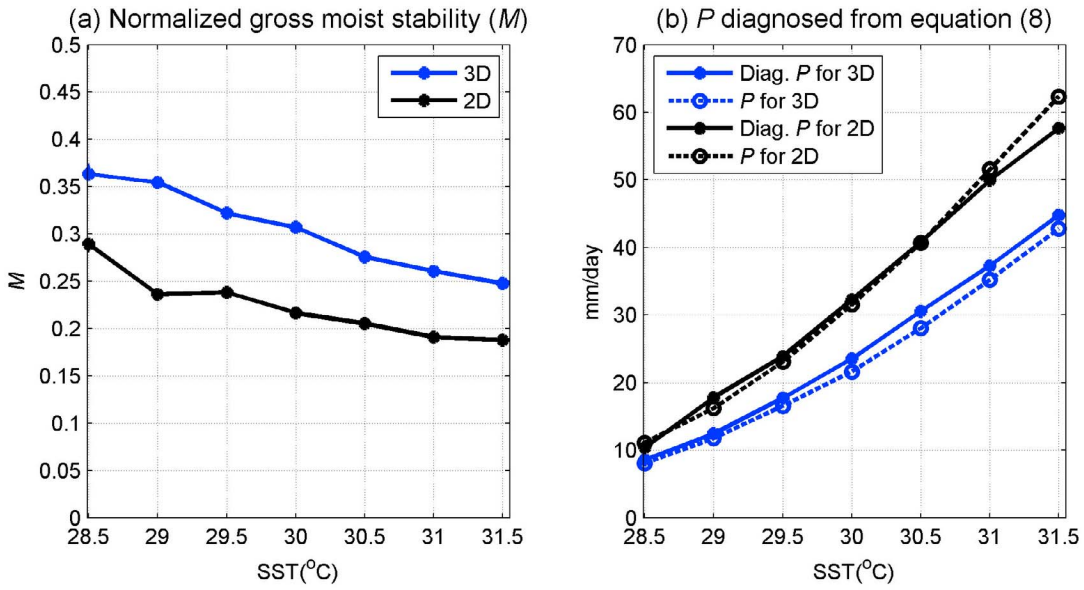

Figure 12. (a) Normalized gross moist stability M estimated using the model output. (b) Daily rain rate (mm/d) diagnosed using equation (8) with estimated M (solid lines) and daily rain rate from model output (dashed lines).

where P, E, H, and Q_R denote precipitation, surface sensible flux, latent flux, and radiative heating and terms in angle brackets ($= \int_{p_0}^{P_T} dp/g$) denote the mass-weighted vertical integral from the bottom to the top of the domain.

[53] In the wet regime, it is useful to consider the following diagnostic relation [*Sobel*, 2007] to understand P,

$$P = \frac{1}{M}(E + H + \langle Q_R \rangle) - \langle Q_R \rangle - H, \tag{8}$$

where M is the normalized gross moist stability, a dimensionless number estimated as $M = \langle \overline{w}(\partial \overline{h}/\partial z) \rangle / \langle \overline{w}(\partial \overline{s}/\partial z) \rangle$, where the overbar indicates time averaging (over whatever time scale we want to compute P) encapsulates the influence of the divergent atmospheric circulation on the moist and dry static energy budgets in the way relevant to precipitation [*Neelin and Held*, 1987]. Given the estimate of M, knowing energy fluxes will allow us to diagnose the precipitation. The parameter M is similar to the "normalized gross moist stability" in the study by *Raymond et al.* [2009], with the minor difference that the denumerator here is the dry static energy divergence rather than the moisture convergence. (Note, however, that *Neelin and Held* [1987] and many subsequent authors have used the notation M for the gross moist stability defined with a different normalization and different dimensions; our M is dimensionless.)

[54] We utilize the relation (8) to estimate precipitation using the modeled energy fluxes and M evaluated from the model output, all sampled every 12 h. The radiation flux from our simple radiative scheme leads to nearly constant radiative cooling of ~145 W/m^2. The surface fluxes increase roughly linearly, as discussed before. Comparing this to the precipitation output directly by the model gives a good idea of the degree to which energy is conserved in the model, as well as that to which fluctuations on time scales shorter than 12 h can be neglected in the budget (as they are in equation (8); i.e., if all quantities individually are time averaged, then the precisely correct equations should have also the time-averaged products of shorter time scale fluctuations in all nonlinear terms). The relative magnitudes of the different terms then provide information about the relative roles of circulation and surface fluxes (radiative cooling again varying little here) in producing the precipitation variations with SST.

[55] Figure 12a shows M, computed from the domain and time-averaged data. Alternatively, we have also diagnosed M by replacing the time-averaged quantities with median values, or by performing time average of instantaneous M, or by taking the median value of instantaneous M. These different estimates yield nearly identical values for all 3-D experiments, while estimates using the time average of instantaneous M show greater variations for the 2-D experiments. This indicates that transients play a greater role in two dimensions, as might have been expected from the other results above.

[56] Generally, the gross moist stability M decreases with SST in the wet regime. This is true in three dimensions over the entire range of SST and in two dimensions for SST > 29.5°C. M decreases gradually from 0.36 at SST = 28.5°C to ~0.25 at SST = 31.5°C for three dimensions. Computations of M holding either WTG vertical velocity or mean moist static energy fixed (not shown) suggest that changes in moist static energy explain almost entirely the variations in M in two dimensions, as might be expected from the self-similarity of W_{wtg} profiles shown in Figure 4. In three dimensions, these calculations suggest that while changes in moist static energy explain much of the M variation with SST, changes in W_{wtg} also play a role despite their smallness.

[57] The values of M in two dimensions are all smaller than those in three dimensions. This indicates higher P in two than in three dimensions given similar surface forcing, as seen from equation (8). Figure 12b shows the

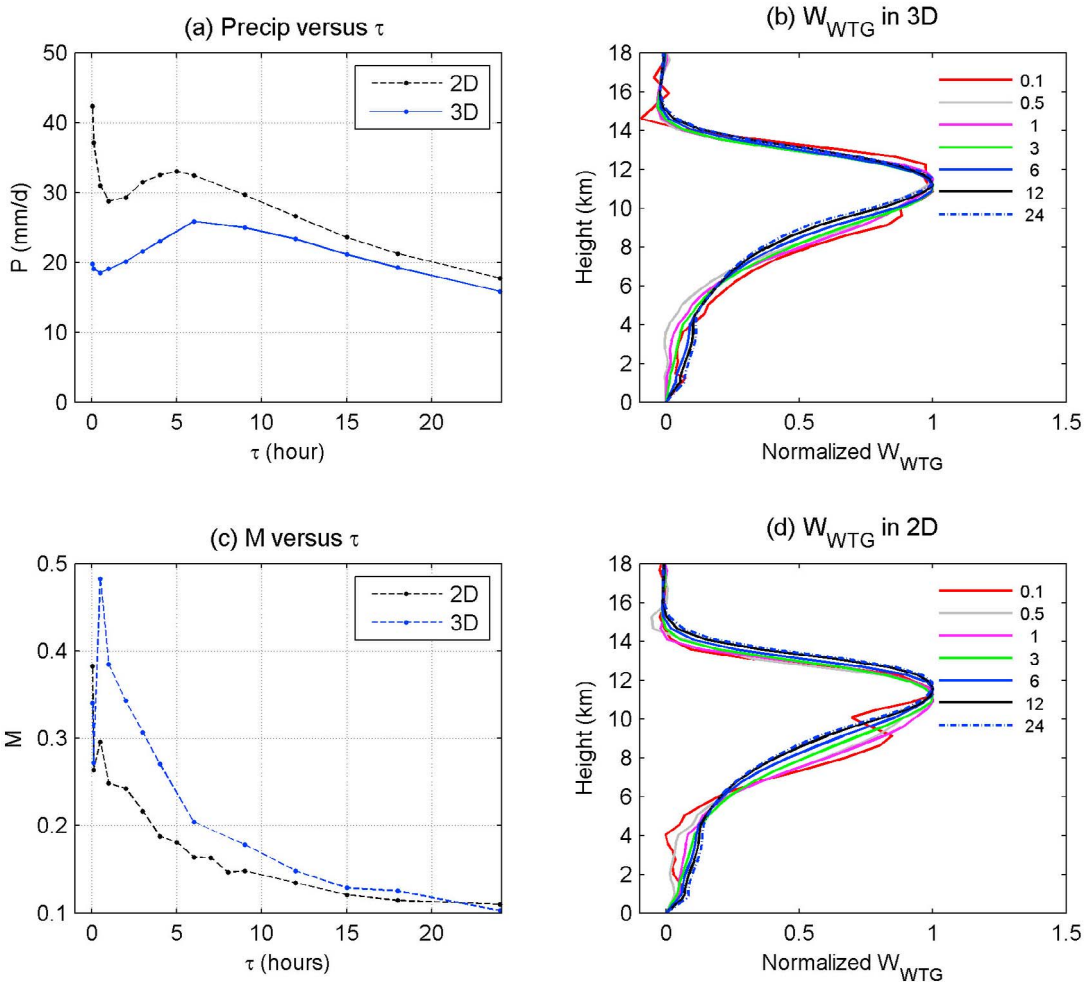

Figure 13. (a) Precipitation versus the relaxation time scale τ at SST = 30°C for 2-D and 3-D experiments. (c) Normalized gross moist stability versus τ. (b and d) Normalized W_{wtg} in two and three dimensions, respectively. For clarity, only the experiments with τ = 0.5, 1, 3, 8, 12, and 24 h are plotted in Figures 13b and 13d.

precipitation computed from equation (8). This diagnosis of P based on the energy budgets is quantitatively close to the actual daily mean precipitation for the 3-D experiments. P is underestimated slightly more at high SST in two dimensions, consistent with the greater role of neglected high-frequency transients.

[58] The smaller values of M in two than in three dimensions are the main reason for the greater P in two dimensions. This can be seen from the budget of precipitation (equation (8)), which states that three factors can contribute to the increase of precipitation with SST in steady state: surface fluxes, radiative cooling, and M. In our experiments, the surface fluxes are slightly smaller in three than in two dimensions (Figure 3), and radiation cooling is nearly the same in two and three dimensions, but M is significantly smaller in two dimensions.

3.7. Sensitivity to WTG Relaxation Time τ

[59] In all experiments discussed above, the Newtonian relaxation time scale τ in equation (1) is 3 h. Here we explore the solution sensitivity to τ. Given the same 2°C SST forcing (SST = 30°C) in both 2-D and 3-D experiments, τ is varied from 3 min to 2 days: 0.05, 0.1, 0.5, 1, 2, 3, 4, 6, 9, 12, 15, 18, 24, and 48 h. Presumably, interaction between convection and WTG vertical velocity W_{wtg} is the strongest in the zero limit of τ and the weakest in the infinity limit. As we show below, at finite τ there is a local minimum and a maximum in the precipitation as a function of τ.

[60] Figure 13a shows that P achieves a maximum at τ = 5–6 h and a minimum at τ = 0.5 h. The local minimum is associated with the large value of gross moist stability (Figure 13c). The local maximum is also seen in previous WTG studies [*Sessions et al.*, 2010 Figure 9; *Kuang*, 2011]. *Kuang* [2011] interpreted the dependence of gross moist stability on horizontal wavelength, a parameter that (squared) plays the same role as τ in our calculations, as potentially responsible for the scale selection in the Madden-Julian oscillation, assuming the dynamics of that mode to be described by "column MSE instability," or (almost equivalently) as a "moisture mode" [*Neelin and Yu*, 1994; *Sobel et al.*, 2001; *Fuchs and Raymond*, 2002; *Sobel and Bretherton*, 2003; *Bretherton et al.*, 2005; *Fuchs and Raymond*, 2005; *Fuchs*

and Raymond, 2007; *Raymond and Fuchs*, 2007; *Raymond and Fuchs*, 2009; *Sugiyama*, 2009a, 2009b; *Maloney et al.*, 2010]. The decrease in P in Figure 13a at large τ is easily understood; the system must return to RCE as τ goes to infinity, and in that limit, the precipitation must return to the value determined by radiative cooling. Consistent with the dependence on horizontal wavelength found by *Kuang* [2011], as τ increases, W_{wtg} becomes less top heavy and gross moist stability decreases (Figure 13c). This is explains the increase of P with τ at small τ shown in Figure 13a. As τ increases to larger values, the decline of P can presumably be understood as the beginning of the approach to the limit as τ goes to infinity. In this limit, the system must approach RCE, implying that surface fluxes balance radiative cooling, surface evaporation balances precipitation, and M becomes undefined as W_{wtg} vanishes. This limit is not yet close at τ = 24 h, but the decrease of surface latent heat flux (not shown) is already sufficient to overcome the decrease in M and cause reduction in P.

[61] Figures 13b and 13d show normalized W_{wtg} in two and three dimensions. As τ is varied, vertical structure in W_{wtg} changes systematically. Below 4 km, W_{wtg} is smaller for small τ than large τ; above 4 km, W_{wtg} is almost independent of τ. In other words, the profile is less top heavy as τ increases, unlike the self-similar behavior of W_{wtg} as SST is varied. This explains the decrease in gross moist stability with τ mentioned above. The change of W_{wtg} with respect to τ is not uniform over the range of τ considered: it is relatively large as τ increases up to 6 h and very small as τ varies from 6 to 24 h. The latter is consistent with the self-similar behavior of W_{wtg} in SST forcing experiments.

[62] The difference between two and three dimensions is evident for all τ values but is largest in the limit $\tau = 0$ and the smallest in the limit $\tau = \infty$.

3.8. Sensitivity to Domain Size

[63] In the results discussed in previous sections, the domain size is 192 km. Here we repeat our 2-D and 3-D experiments in smaller domains: 128 and 64 km, respectively. In both 2-D and 3-D experiments, varying domain size seems have little impact on the equilibrated precipitation (not shown). On the other hand, precipitation in two dimensions remains clearly different from that in three dimensions, indicating that the comparisons between two and three dimensions are robust.

4. Conclusions

[64] In this study, equilibrated tropical convection is explored using a cloud-resolving model. The weak temperature gradient approximation is used to parameterize the coupling between explicitly resolved convection and large-scale motion. Sea surface temperature is varied while other parameters, including the target temperature profile toward which the horizontal mean free tropospheric temperature is relaxed, are held fixed. Model integrations are performed with both 2-D and 3-D geometry. The primary findings are as follows.

[65] 1. As in previous studies with parameterized convection, and as expected from basic considerations, precipitation increases with relative sea surface temperature. The increase is not independent of geometry, however. While the RCE states in two and three dimensions are similar, precipitation increases more rapidly in two than in three dimensions as SST is increased above the RCE value. As an example, given an SST increase of 2 K above the RCE value, P is 60% more in two than in three dimensions.

[66] 2. When the time scale at which the horizontal mean free tropospheric temperature is relaxed to the target profile is held fixed at a small value (e.g., 3 h), the shape of the WTG vertical velocity profile is remarkably invariant with SST (as long as SST is above the RCE value), although the magnitude varies strongly with SST. Cloud fraction and convective mass flux show a lesser degree of self-similarity with SST.

[67] 3. As might be expected given the precipitation results, both the WTG vertical velocity, and other measures of the intensity of the resolved convection, such as convective mass fluxes and cloud fraction, increase more rapidly in two than in three dimensions. We expect that the difference between two and three dimensions may be attributed to differences in the buoyancy of PBL parcels and entrainment. Entrainment is not quantified in this study but is expected to be weaker (thus diluting updraft buoyancy less) in two than in three dimensions. We do analyze the distributions of near-surface equivalent potential temperature and show that larger values occur more frequently in two than in three dimensions.

[68] 4. Precipitation as a function of column-integrated relative humidity, when results from all model integrations are plotted together, shows the expected qualitative behavior, with no precipitation when CRH is below a threshold value and a rapid increase above that. However, within each individual model integration, CRH and precipitation show a clear negative correlation as both vary within narrow ranges of their respective quasi-equilbrium states. This is presumably indicative of the negative feedback that maintains the tight coupling observed over the larger ranges filled by the ensemble of model integrations. This behavior is found in both two and three dimensions.

[69] 5. An analysis of the moist static energy budget shows that the normalized gross moist stability is smaller in two than in three dimensions. This is consistent with the greater precipitation in two dimensions, as it leads to greater moisture convergence for the same surface evaporation. Surface evaporation as a function of SST is very similar in two and three dimensions. The normalized gross moist stability decreases smoothly with SST but remains positive.

[70] 6. When the time scale at which the horizontal mean free tropospheric temperature is varied, the shape of the WTG vertical velocity profile changes. At a longer relaxation time, corresponding to larger warming of the upper troposphere in response to convection, the WTG vertical velocity in the lower troposphere increases while the upper tropospheric peak narrows. To the extent that these results can be compared with those of *Kuang* [2011], the lower tropospheric change is consistent while the upper one is inconsistent. These differences likely result from the different formulations of WTG in the two models and are worthy of further investigation. However, the overall decrease of top heaviness, and gross moist stability, with relaxation time is qualitatively consistent with the results of *Kuang* [2011], who proposed this as a mechanism for the scale selection of the Madden-Julian oscillation.

[71] **Acknowledgments.** This work was supported by NSF grant AGS-1008847 and NASA grant NNX07AP74A. We thank David Raymond and Zhiming Kuang for their comments, which were very helpful in improving this manuscript. We also thank Joseph Galewsky for discussions during the early phase of this work. Discussions with Chris Bretherton and Hamish Ramsay were also helpful. We thank NCAR's Computational and Information Systems Laboratory, where part of the experiments were performed.

References

Back, L. E., and C. S. Bretherton (2006), Geographic variability in the export of moist static energy and vertical motion profiles in the tropical Pacific, *Geophys. Res. Lett.*, *33*, L17810, doi:10.1029/2006GL026672.

Back, L. E., and C. S. Bretherton (2009), A simple model of climatological precipitation and vertical motion patterns over the tropical oceans, *J. Clim.*, *22*, 6477–6497, doi:10.1175/2009JCLI2393.1.

Bergman, J., and P. D. Sardeshmukh (2004), Dynamic stabilization of atmospheric single column models, *J. Clim.*, *17*, 1004–1021, doi:10.1175/1520-0442(2004)017<1004:DSOASC>2.0.CO;2.

Blossey, P. N., C. S. Bretherton, and M. C. Wyant (2009), Understanding subtropical low cloud response to a warmer climate in a superparameterized climate model. Part II: Column modeling with a cloud-resolving model, *J. Adv. Model. Earth Syst.*, *1*, 14 pp., doi:10.3894/JAMES.2009.1.8.

Bretherton, C. S., and P. K. Smolarkiewicz (1989), Gravity waves, compensating subsidence, and detrainment around cumulus clouds, *J. Atmos. Sci.*, *46*, 740–759, doi:10.1175/1520-0469(1989)046<0740:GWCSAD>2.0.CO;2.

Bretherton, C. S., M. E. Peters, and L. E. Back (2004), Relationships between water vapor path and precipitation over the tropical oceans, *J. Clim.*, *17*, 1517–1528, doi:10.1175/1520-0442(2004)017<1517:RBWVPA>2.0.CO;2.

Bretherton, C. S., P. N. Blossey, and M. Khairoutdinov (2005), An energy-balance analysis of deep convective self-aggregation above uniform SST, *J. Atmos. Sci.*, *62*, 4273–4292, doi:10.1175/JAS3614.1.

Chen, S.-H., and W.-Y. Sun (2002), A one-dimensional time dependent cloud model, *J. Meteorol. Soc. Jpn.*, *80*, 99–118, doi:10.2151/jmsj.80.99.

Chiang, J. C. H., and A. H. Sobel (2002), Tropical tropospheric temperature variations caused by ENSO and their influence on the remote tropical climate, *J. Clim.*, *15*, 2616–2631, doi:10.1175/1520-0442(2002)015<2616:TTTVCB>2.0.CO;2.

Emanuel, K. A. (1995), The behavior of a simple hurricane model using a convective scheme based on subcloud-layer entropy equilibrium, *J. Sci.*, *52*, 3960–3968, doi:10.1175/1520-0469(1995)052<3960:TBOASH>2.0.CO;2.

Fuchs, Z., and D. J. Raymond (2002), Large-scale modes of a nonrotating atmosphere with water vapor and cloud-radiation feedbacks, *J. Atmos. Sci.*, *59*, 1669–1679, doi:10.1175/1520-0469(2002)059<1669:LSMOAN>2.0.CO;2.

Fuchs, Z., and D. J. Raymond (2005), Large-scale modes in a rotating atmosphere with radiative-convective instability and WISHE, *J. Atmos. Sci.*, *62*, 4084–4094, doi:10.1175/JAS3582.1.

Fuchs, Z., and D. J. Raymond (2007), A simple, vertically resolved model of tropical disturbances with a humidity closure, *Tellus, Ser. A*, *59*, 344–354, doi:10.1111/j.1600-0870.2007.00230.x.

Grabowski, W. W., X. Wu, M. W. Moncrieff, and W. D. Hall (1998), Cloud-resolving modeling of cloud systems during phase III of GATE. Part II: Effects of resolution and the third spatial dimension, *J. Atmos. Sci.*, *55*, 3264–3282, doi:10.1175/1520-0469(1998)055<3264:CRMOCS>2.0.CO;2.

Held, I. M., R. S. Hemler, and V. Ramaswamy (1993), Radiative-convective equilibrium with explicit two-dimensional moist convection, *J. Atmos. Sci.*, *50*, 3909–3927, doi:10.1175/1520-0469(1993)050<3909:RCEWET>2.0.CO;2.

Holloway, C. H., and J. D. Neelin (2009), Moisture vertical structure, column water vapor, and tropical deep convection, *J. Atmos. Sci.*, *66*, 1665–1683, doi:10.1175/2008JAS2806.1.

Hong, S.-Y., and H.-L. Pan (1996), Nonlocal boundary layer vertical diffusion in a Medium-Range Forecast model, *Mon. Weather Rev.*, *124*, 2322–2339, doi:10.1175/1520-0493(1996)124<2322:NBLVDI>2.0.CO;2.

Hong, S.-Y., Y. Noh, and J. Dudhia (2006), A new vertical diffusion package with an explicit treatment of entrainment processes, *Mon. Weather Rev.*, *134*, 2318–2341, doi:10.1175/MWR3199.1.

Khairoutdinov, M., D. A. Randall, and C. DeMott (2005), Simulations of the atmospheric general circulation using a cloud-resolving model as a superparameterization of physical processes, *J. Atmos. Sci.*, *62*, 2136–2154, doi:10.1175/JAS3453.1.

Klemp, J. B., J. Dudhia, and A. Hassiotis (2008), An upper gravity wave absorbing layer for NWP applications, *Mon. Weather Rev.*, *136*, 3987–4004, doi:10.1175/2008MWR2596.1.

Kuang, Z. (2008), Modeling the interaction between cumulus convection and linear waves using a limited domain cloud system resolving model, *J. Atmos. Sci.*, *65*, 576–591, doi:10.1175/2007JAS2399.1.

Kuang, Z. (2011), The wavelength dependence of the gross moist stability and the scale selection in the instability of column integrated moist static energy, *J. Atmos. Sci.*, *68*, 61–74, doi:10.1175/2010JAS3591.1.

Lin, Y.-L., R. D. Farley, and H. D. Orville (1983), Bulk parameterization of the snow field in a cloud model, *J. Clim. Appl. Meteorol.*, *22*, 1065–1092, doi:10.1175/1520-0450(1983)022<1065:BPOTSF>2.0.CO;2.

Maloney, E. D., A. H. Sobel, and W. Hannah (2010), Intraseasonal variability in an aquaplanet general circulation model, *J. Adv. Model. Earth Syst.*, *2*, 24 pp., doi:10.3894/JAMES.2010.2.5.

Mapes, B. E. (2004), Sensitivities of cumulus ensemble rainfall in a cloud-resolving model with parameterized large-scale dynamics, *J. Atmos. Sci.*, *61*, 2308–2317, doi:10.1175/1520-0469(2004)061<2308:SOCRIA>2.0.CO;2.

Muller, C. J., L. E. Back, P. A. O'Gorman, and K. A. Emanuel (2009), A model for the relationship between tropical precipitation and column water vapor, *Geophys. Res. Lett.*, *36*, L16804, doi:10.1029/2009GL039667.

Neelin, J. D., and I. M. Held (1987), Modeling tropical convergence based on the moist static energy budget, *Mon. Weather Rev.*, *115*, 3–12, doi:10.1175/1520-0493(1987)115<0003:MTCBOT>2.0.CO;2.

Neelin, J. D., and J. Y. Yu (1994), Modes of tropical variability under convective adjustment and the Madden-Julian oscillation. 1. Analytical theory, *J. Atmos. Sci.*, *51*, 1876–1894, doi:10.1175/1520-0469(1994)051<1876:MOTVUC>2.0.CO;2.

Neelin, J. D., O. Peters, J. W.-B. Lin, K. Hales, and C. E. Holloway (2009), Rethinking convective quasi-equilibrium: Observational constraints for stochastic convective schemes in climate models, in *Stochastic Physics and Climate Modelling*, edited by T. N. Palmer and P. D. Williams, pp. 396–423, Cambridge Univ. Press, Cambridge, U. K.

Noh, Y., W. G. Cheon, S.-Y. Hong, and S. Raasch (2003), Improvement of the K-profile model for the planetary boundary layer based on large eddy simulation data, *Boundary Layer Meteorol.*, *107*, 401–427, doi:10.1023/A:1022146015946.

Pauluis, O., and S. Garner (2006), Sensitivity of radiative–convective equilibrium simulations to horizontal resolution, *J. Atmos. Sci.*, *63*, 1910–1923, doi:10.1175/JAS3705.1.

Petch, J. C., P. N. Blossey, and C. S. Bretherton (2008), Differences in the lower troposphere in two- and three-dimensional cloud-resolving model simulations of deep convection, *Q. J. R. Meteorol. Soc.*, *134*, 1941–1946.

Peters, O., and J. D. Neelin (2006), Critical phenomena in atmospheric precipitation, *Nat. Phys.*, *2*, 393–396, doi:10.1038/nphys314.

Phillips, V. T., and L. J. Donner (2006), Cloud microphysics, radiation, and vertical velocities in two- and three-dimensional simulations of deep convection, *Q. J. R. Meteorol. Soc.*, *132*, 3011–3033, doi:10.1256/qj.05.171.

Ramsay, H. A., and A. H. Sobel (2011), The effects of relative and absolute sea surface temperature on tropical cyclone potential intensity using a single column model, *J. Clim.*, *24*, 183–193, doi:10.1175/2010JCLI3690.1.

Raymond, D. J. (1995), Regulation of moist convection over the west Pacific warm pool, *J. Atmos. Sci.*, *52*, 3945–3959, doi:10.1175/1520-0469(1995)052<3945:ROMCOT>2.0.CO;2.

Raymond, D. J. (2000), Thermodynamic control of tropical rainfall, *Q. J. R. Meteorol. Soc.*, *126*, 889–898, doi:10.1256/smsqj.56405.

Raymond, D. J. (2007), Testing a cumulus parameterization with a cumulus ensemble model in weak temperature gradient mode, *Q. J. R. Meteorol. Soc.*, *133*, 1073–1085, doi:10.1002/qj.80.

Raymond, D. J., and Z. Fuchs (2007), Convectively coupled gravity and moisture modes in a simple atmospheric model, *Tellus, Ser. A*, *59*, 627–640, doi:10.1111/j.1600-0870.2007.00268.x.

Raymond, D. J., and Z. Fuchs (2009), Moisture modes and the Madden-Julian oscillation, *J. Clim.*, *22*, 3031–3046, doi:10.1175/2008JCLI2739.1.

Raymond, D. J., and S. L. Sessions (2007), Evolution of convection during tropical cyclogenesis, *Geophys. Res. Lett.*, *34*, L06811, doi:10.1029/2006GL028607.

Raymond, D. J., and X. Zeng (2005), Modelling tropical atmospheric convection in the context of the weak temperature gradient approximation, *Q. J. R. Meteorol. Soc.*, *131*, 1301–1320, doi:10.1256/qj.03.97.

Raymond, D. J., S. L. Sessions, A. H. Sobel, and Z. Fuchs (2009), The mechanics of gross moist stability. *J. Adv. Model. Earth Syst.*, *1*, 20 pp., doi:10.3894/JAMES.2009.1.9.

Robe, F. R., and K. A. Emanuel (1996), Dependence of tropical convection on radiative forcing, *J. Atmos. Sci.*, *53*, 3265–3275, doi:10.1175/1520-0469(1996)053<3265:MCSSIF>2.0.CO;2.

Rutledge, S. A., and P. V. Hobbs (1984), The mesoscale and microscale structure and organization of clouds and precipitation in midlatitude cyclones. XII: A diagnostic modeling study of precipitation development in narrow cloud-frontal rainbands, *J. Atmos. Sci.*, *41*, 2949–2972, doi:10.1175/1520-0469(1984)041<2949:TMAMSA>2.0.CO;2.

Sessions, S., D. J. Raymond, and A. H. Sobel (2010), Multiple equilibria in a cloud-resolving model, *J. Geophys. Res.*, *115*, D12110, doi:10.1029/2009JD013376.

Shaevitz, D. A., and A. H. Sobel (2004), Implementing the weak temperature gradient approximation with full vertical structure, *Mon. Weather Rev.*, *132*, 662–669, doi:10.1175/1520-0493(2004)132<0662:ITWTGA>2.0.CO;2.

Skamarock, W. C., J. B. Klemp, J. Dudhia, D. O. Gill, D. M. Barker, M. G. Duda, X. Huang, W. Wang, and J. G. Powers (2008), A description of the Advanced Research WRF version 3, *Tech. Note NCAR/TN-475+STR*, 125 pp., Natl. Cent. for Atmos. Res., Boulder, Colo.

Sobel, A. H. (2007), Simple models of ensemble-averaged precipitation and surface wind, given the SST, in *The Global Circulation of the Atmosphere*, edited by T. Schneider and A. H. Sobel, pp. 219–251, Princeton Univ. Press, Princeton, N. J.

Sobel, A. H., and G. Bellon (2009), The effect of imposed drying on parameterized deep convection, *J. Atmos. Sci.*, *66*, 2085–2096, doi:10.1175/2008JAS2926.1.

Sobel, A. H., and C. S. Bretherton (2000), Modeling tropical precipitation in a single column, *J. Clim.*, *13*, 4378–4392, doi:10.1175/1520-0442(2000)013<4378:MTPIAS>2.0.CO;2.

Sobel, A. H., and C. S. Bretherton (2003), Large-scale waves interacting with deep convection in idealized mesoscale model simulations, *Tellus, Ser. A*, *55*, 45–60.

Sobel, A. H., J. Nilsson, and L. M. Polvani (2001), The weak temperature gradient approximation and balanced tropical moisture waves, *J. Atmos. Sci.*, *58*, 3650–3665, doi:10.1175/1520-0469(2001)058<3650:TWTGAA>2.0.CO;2.

Sobel, A. H., I. M. Held, and C. S. Bretherton (2002), The ENSO signal in tropical tropospheric temperature, *J. Clim.*, *15*, 2702–2706, doi:10.1175/1520-0442(2002)015<2702:TESITT>2.0.CO;2.

Sobel, A. H., G. Bellon, and J. T. Bacmeister (2007), Multiple equilibria in a single-column model of the tropical atmosphere, *Geophys. Res. Lett.*, *34*, L22804, doi:10.1029/2007GL031320.

Stephens, G. L., S. C. van den Heever, and L. Pakula (2008), Radiative–convective feedbacks in idealized states of radiative–convective equilibrium, *J. Atmos. Sci.*, *65*(12), 3899–3916, doi:10.1175/2008JAS2524.1.

Sugiyama, M. (2009a), The moisture mode in the quasi-equilibrium tropical circulation model. Part I: Analysis based on the weak temperature gradient approximation, *J. Atmos. Sci.*, *66*, 1507–1523, doi:10.1175/2008JAS2690.1.

Sugiyama, M. (2009b), The moisture mode in the quasi-equilibrium tropical circulation model. Part II: Nonlinear behavior on an equatorial beta plane, *J. Atmos. Sci.*, *66*, 1525–1542, doi:10.1175/2008JAS2691.1.

Tompkins, A. M. (2000), The impact of dimensionality on long-term cloud-resolving model simulations, *Mon. Weather Rev.*, *128*, 1521–1535, doi:10.1175/1520-0493(2000)128<1521:TIODOL>2.0.CO;2.

Tompkins, A. M. (2001), Organization of tropical convection in low vertical wind shears: The role of cold pools, *J. Atmos. Sci.*, *58*, 1650–1672, doi:10.1175/1520-0469(2001)058<1650:OOTCIL>2.0.CO;2.

Troen, I., and L. Mahrt (1986), A simple model of the atmospheric boundary layer: Sensitivity to surface evaporation, *Boundary Layer Meteorol.*, *37*, 129–148, doi:10.1007/BF00122760.

Vecchi, G. A., and B. J. Soden (2007), Effect of remote sea surface temperature change on tropical cyclone potential intensity, *Nature*, *450*, 1066–1070, doi:10.1038/nature06423.

Wu, X., and S. Guimond (2006), Two- and three-dimensional cloud-resolving model simulations of the mesoscale enhancement of surface heat fluxes by precipitating deep convection, *J. Clim.*, *19*, 139–149, doi:10.1175/JCL3610.1.

Zeng, X., et al. (2007), Evaluating clouds in long-term cloud-resolving model simulations with observational data, *J. Atmos. Sci.*, *64*, 4153–4177, doi:10.1175/2007JAS2170.1.

A. H. Sobel and S. Wang, Department of Applied Physics and Applied Mathematics, Columbia University, 500 West 120th Street, New York, NY 10027, USA. (sw2526@columbia.edu)